DOI: 10.1590/2317-4889201820180046

ARTICLE

First Lu-Hf, $\delta^{18}O$ and trace elements in zircon signatures from the Statherian Espinhaço anorogenic province (Eastern Brazil): geotectonic implications of a silicic large igneous province

Joana Reis Magalhães[1,2,3]*, Antonio Pedrosa-Soares[1], Ivo Dussin[4], Othmar Müntener[2], Marco Aurélio P. Pinheiro[3], Luiz Carlos da Silva[3], Luiz Guilherme Knauer[1], Anne-Sophie Bouvier[2], Lukas Baumgartner[2]

ABSTRACT: *The Espinhaço rift system encompasses taphrogenetic events from the Statherian to Tonian in the São Francisco-Congo (SFC) paleocontinent. The magmatism is represented mainly by metamorphosed anorogenic granites and rhyolites with subordinate amphibolites. Zircon U–Pb (LA-ICPMS and SHRIMP) ages from felsic (1748 ± 3 Ma and 1740 ± 8 Ma) and mafic (1725 ± 4 Ma) rock samples, coupled with previous studies suggest that the Espinhaço igneous province erupted from ca. 1.79 Ga to ca. 1.70 Ga. The felsic rocks show characteristics of A-type magmas. The negative εHf(t) data for meta-rhyolite zircons (-12.32 to -17.58), the moderate $\delta^{18}O$ values (7.02 to 7.98) and the REE patterns suggest crustal melting related to an extensional environment. The mafic rock shows negative values of εHf(t) in zircons (-4.05 to -8.25) and moderate $\delta^{18}O$ values (5.56 to 7.87). The results disclose a basaltic magmatism in continental intraplate setting whose parental magma could have been derived from the subcontinental lithospheric mantle with contamination of crustal material. These data coupled with coeval Espinhaço magmatism and mafic dyke swarms found to the south of the Espinhaço rift system reinforce the evidence of a long-lived Statherian silicic large igneous province (SLIP) on the SFC paleocontinental block.*

KEYWORDS: *Statherian magmatism; taphrogenic event; Espinhaço rift; São Francisco paleocontinent.*

INTRODUCTION

The outstanding development of chemical and isotopic analysis on zircon grains enhanced the understanding of nature, evolution and source of igneous rocks related to distinct tectonic environments and its geodynamic processes. Because zircon grains are able to record multiple geological events, through its morpho-chemical modifications, numerous investigations, as U-Pb and Lu-Hf systematics, as well as $\delta^{18}O$ and REE abundances, have been focused on relating temporal evolution of the crust and the lithospheric mantle (Hoskin and Schaltegger 2003, Harley and Kelly 2007). Even some representative zircon samples can disclose new findings and test previous hypothesis suggested by lithochemical and whole-rock isotopic methods. Such analytical methods of zircon spot analysis are here presented on samples of felsic and mafic rocks from the Espinhaço igneous province which rift-related anorogenic nature has been suggested since the early 1990's, based only on lithochemical data from felsic rocks (Chemale Jr. 1987, Dussin 1994, Fernandes 2001).

[1]Programa de Pós-Graduação em Geologia, Centro de Pesquisas Professor Manoel Teixeira da Costa, Universidade Federal de Minas Gerais – Belo Horizonte (MG), Brazil. *E-mails: jomagalhaes@gmail.com, pedrosasoares@gmail.com, gknauer@gmail.com*

[2]Institute of Earth Sciences, University of Lausanne – Geópolis, Quartier Mouline, Lausanne, Switzerland. *E-mails: othmar.muntener@unil.ch, anne-sophie.bouvier@unil.ch, lukas.baumgartner@unil.ch*

[3]Geological Survey of Brazil – Belo Horizonte (MG), Brazil. *E-mail: marcopiacentini@gmail.com, luiz.silva@cprm.gov.br*

[4]Faculdade de Geologia, Universidade do Estado do Rio de Janeiro – Rio de Janeiro (RJ), Brazil. *E-mail: ivodusin@yahoo.com.br*

*Corresponding author

Manuscript ID: 20180046. **Received on:** 04/17/2018. **Approved on:** 08/22/2018.

The São Francisco-Congo (SFC) paleocontinental block (Fig. 1A), amalgamated in the Rhyacian — Orosirian boundary (ca. 2.05 Ga), experienced a series of rifting events from the Statherian to Cryogenian (Pedrosa-Soares and Alkmim 2011, Chemale Jr. *et al.* 2012a, Danderfer *et al.* 2015, Heilbron *et al.* 2017). The oldest among those taphrogenic events took place in Early Statherian time, around 1.75–1.70 Ga, cutting across the São Francisco block in Central-Eastern Brazil, and culminating with the opening of the extensive N-S-trending Espinhaço basin system associated with abundant acid magmatism (Fig. 1B).

To the east of the main exposure region of the Southern Espinhaço rift, Statherian felsic magmatism is also registered in the Guanhães Archean basement block (Fig. 1B), where large A-type granitic intrusions and rhyolitic volcanism have been referred to for decades (*e.g.*, Dussin 1994, Fernandes 2001). These meta-rhyolites are found in close association with meta-mafic rocks (ortho-amphibolites), both lacking detailed analytical studies. Therefore, they are now the first bimodal suite related to the Espinhaço rift characterized with robust analytical data.

Besides new U-Pb (LA-MC-ICP-MS and SHRIMP) zircon ages, lithochemical and mineral chemistry data, we present the first Lu-Hf, $\delta^{18}O$ and trace elements in zircon data for the mafic and felsic magmatism related to the Espinhaço rift system. Our robust dataset, together with a thorough data compilation from the literature, demonstrate the rift-related bimodal nature of the Espinhaço magmatic province. Furthermore, it supports the role of subcontinental lithospheric mantle on the petrogenesis of these anorogenic rock suite. Finally, we discuss paleotectonic correlations concerning the São Francisco paleocontinental block, envisaging the Statherian Espinhaço magmatic event as part of a silicic large igneous province (SLIP).

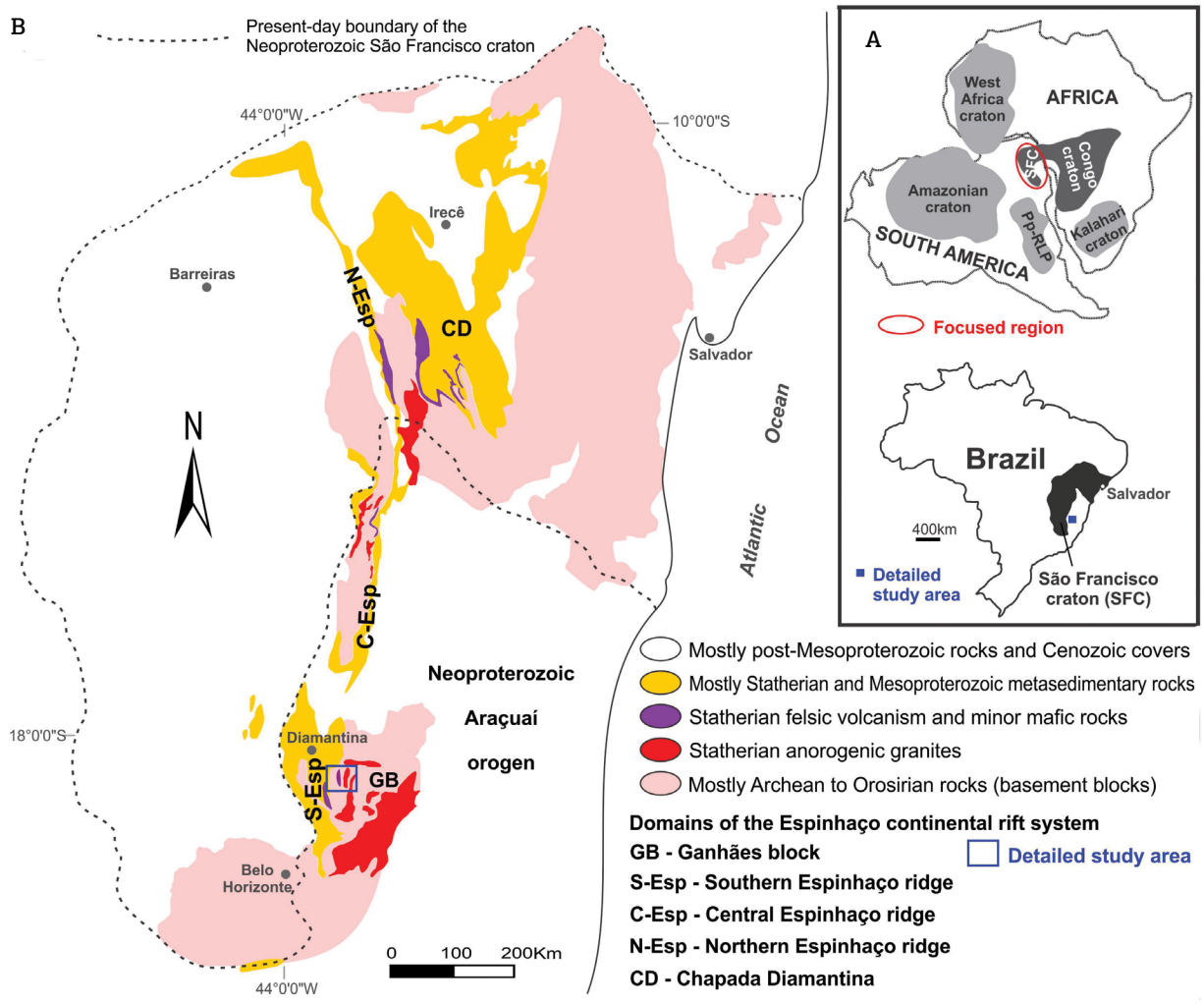

Figure 1. (A) Geotectonic configuration of the São Francisco–Congo craton in the context of West Gondwana (after Alkmim *et al.* 2006). (B) Simplified geological map highlighting the Espinhaço rift system and the Guanhães block in the eastern border of the São Francisco Craton. Modified from Alkmim (2004) and Pinto and Silva (2014).

GEOLOGICAL SETTING

The Espinhaço basin system extends for about 1.200 km along the N-S direction, cutting across the São Francisco paleocontinental block, and can be subdivided into five domains, namely: the Southern Espinhaço ridge, Guanhães block, Central Espinhaço ridge, Northern Espinhaço ridge, and the Chapada Diamantina (*i.e.*, Diamantina plateau) domains (Fig. 1B). While the Northern Espinhaço ridge and Chapada Diamantina domains were mostly preserved from orogenic processes within the São Francisco craton, the Southern and Central Espinhaço ridge domains and Guanhães block were involved in the Brasiliano orogeny within the Neoproterozoic Araçuaí orogen, where they were being mostly metamorphosed in the greenschist facies but locally reaching upper amphibolite facies metamorphism (Pedrosa-Soares *et al*. 2011, Alkmim *et al*. 2017, Cruz and Alkmim 2017). The Espinhaço Supergroup is mostly composed of siliciclastic sequences and magmatic rocks, with minor carbonate rocks, associated with three taphrogenic events that occurred during the Statherian (ca. 1.8–1.68 Ga), Calymmian–Ectasian (ca. 1.6–1.38 Ma) and Stenian (ca. 1.18 Ma) (Pedrosa-Soares and Alkmim 2011, Chemale Jr. *et al*. 2012a, Guadagnin *et al*. 2015, and references therein).

Located to the east of the Southern Espinhaço ridge domain (Fig. 1B), the Guanhães block stands out as a portion of the São Francisco paleocontinental region reworked within the Araçuaí Neoproterozoic orogen (Alkmim *et al*. 2006, 2017, Noce *et al*. 2007a, Silva *et al*. 2011, 2016). The Guanhães block encompasses Archean TTG migmatitic gneisses and associated granites, locally covered by Siderian to Neoproterozoic supracrustal successions, as well as a voluminous Statherian granitic intrusions and meta-ultramafic and meta-mafic rocks of unknown age (Noce *et al*. 2007a, Silva *et al*. 2016, Teixeira *et al*. 2017). Zircon U-Pb (SHRIMP) ages between 3150 Ma and 2710 Ma constrain the magmatic crystallization of both gneiss protoliths and granitoids that also show local metamorphic overprints around 2000 Ma and 570–500 Ma (Silva *et al*. 2011, 2016, Peixoto *et al*. 2015, Barrote 2016).

The Statherian magmatism, aim of this paper, mostly includes anorogenic meta-granites and meta-rhyolites, and minor meta-mafic rocks (Brito Neves *et al*. 1979, Dussin 1994, 2017). The meta-granitic rocks display a wide age spectrum, around 1790–1700 Ma and are represented by the Borrachudos, Catolé and Lagoa Real suites, located in the Guanhães block, Central and Northern Espinhaço domains, respectively (Turpin *et al*. 1988, Pimentel *et al*. 1994, Dussin *et al*. 2000, Fernandes 2001, Costa 2013). Meta-rhyolites dated around 1750 Ma, 1735 Ma and 1710 Ma suggest distinct pulses of felsic volcanism along the Espinhaço system (Machado *et al*. 1989, Babinski *et al*. 1994, Schobbenhaus *et al*. 1994, Danderfer *et al*. 2009, 2015). Statherian meta-mafic rocks dated between 1750 Ma and 1700 Ma occur in the Southern and Central Espinhaço ridge domains (Dussin 1994, Chemale *et al*. Jr. 2012a, Bezerra-Neto 2016, Silva 2016, Moreira 2017). Typical sedimentary rift deposits filled the Statherian Espinhaço basin system. They include sandstones, rudites and pelites related to alluvial fan, braided fluvial and lacustrine environments, with maximum depositional ages between 1.80 Ga and 1.68 Ga (Martins-Neto 2000, Chemale Jr. *et al*. 2012a, Santos *et al*. 2013, Danderfer *et al*. 2015).

In the Guanhães block, where our detailed study area is located, the N-S–trending Alto Rio Guanhães unit comprises a metavolcano-sedimentary rock assemblage tectonically imbricated with the Archean basement, the Guanhães Group and the Statherian meta-granites (Fig. 2). Firstly recognized by Danderfer and Meireles (1987), the Alto Rio Guanhães unit records metamorphosed rocks from the greenschist to the amphibolite facies. The eastern portion of this unit is mostly composed by mafic schists and ortho-amphibolites, representing basic volcanic rocks and associated intrusive mafic bodies, with minor meta-rhyolites and metasedimentary rocks. The western portion mostly comprises quartzites, ferruginous quartzites, pelitic schists, calcsilicate rocks and iron formations, associated with meta-mafic rocks and meta-rhyolites (Fig. 2). Some meta-ultramafic bodies, mostly composed of tremolite-talc schists, are also found within the Alto Rio Guanhães unit.

RESULTS

Samples were collected from representative outcrops of the Alto Rio Guanhães unit and Borrachudos suite. The samples are free of weathering and hydrothermal alteration. We selected samples of mafic (sample J02: 18º38'13"S, 43º12'50"W) and rhyolitic (sample J03: 18º36'15"S, 43º12'52"W) rocks for LA-ICPMS and SIMS isotopic analysis on zircon grains. One sample of a typical syenogranite of the Borrachudos suite, collected from the Açucena pluton (LC40: 18º49'19"S, 42º09'14"W), was selected for zircon U-Pb SHRIMP analyses. Appendix A presents the descriptions of the analytical methods applied in the following sections.

Sample petrography and mineral chemistry

The samples selected for detailed studies are metamorphosed mafic and felsic rocks from the Alto Rio Guanhães unit, and meta-granites of the Borrachudos suite. The mafic rocks are fine- to coarse-grained ortho-amphibolites, representing

volcanic/subvolcanic and plutonic rocks of basaltic composition. The felsic samples include volcanic to subvolcanic rocks of rhyolitic composition and related granites. Mineral chemistry data tables are found in the Supplementary Table A1.

Mafic rocks

The ortho-amphibolites are fine- to coarse-grained rocks, essentially composed of hornblende and plagioclase (Fig. 3A and 3C). The main accessory minerals are quartz, titanite, epidote, apatite and ilmenite. Amphibole is largely dominant (up to 70% in modal content), forming granonematoblastic, stretched, rotated and/or sigmoidal grains along the regional foliation (Fig. 3B). It also exhibits a mottled texture outlined by fine-grained quartz inclusions with interlobate boundaries, suggesting statically recrystallization of exsolved silica. Decussated overgrown amphiboles imprint the anastomosed regional foliation and obliterate previous textures. Amphibole commonly shows zoned crystals, varying from

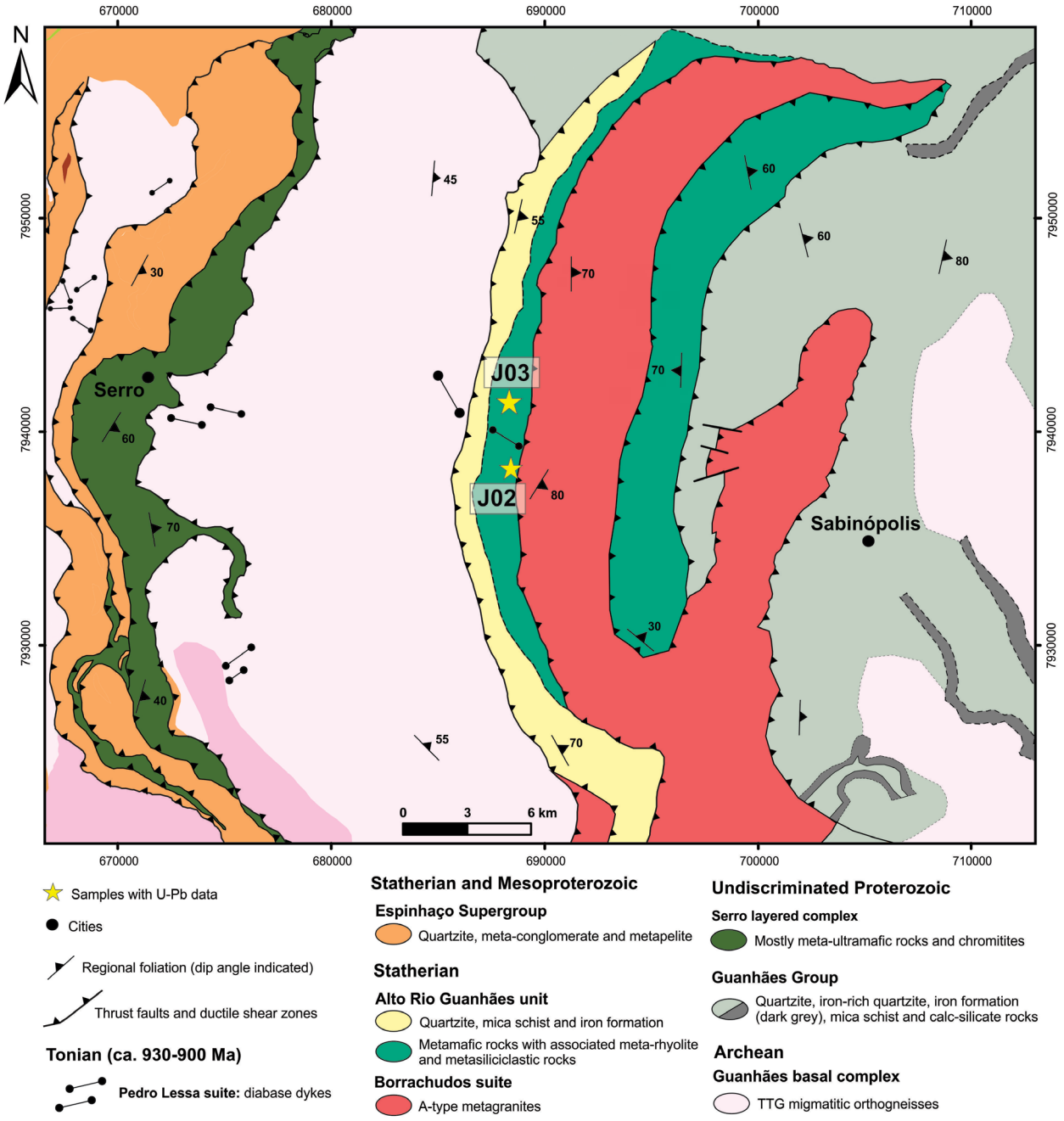

Figure 2. Simplified geologic map of northern region of the Guanhães block and southern area of the Espinhaço Ridge (modified from Pinto and Silva 2014).

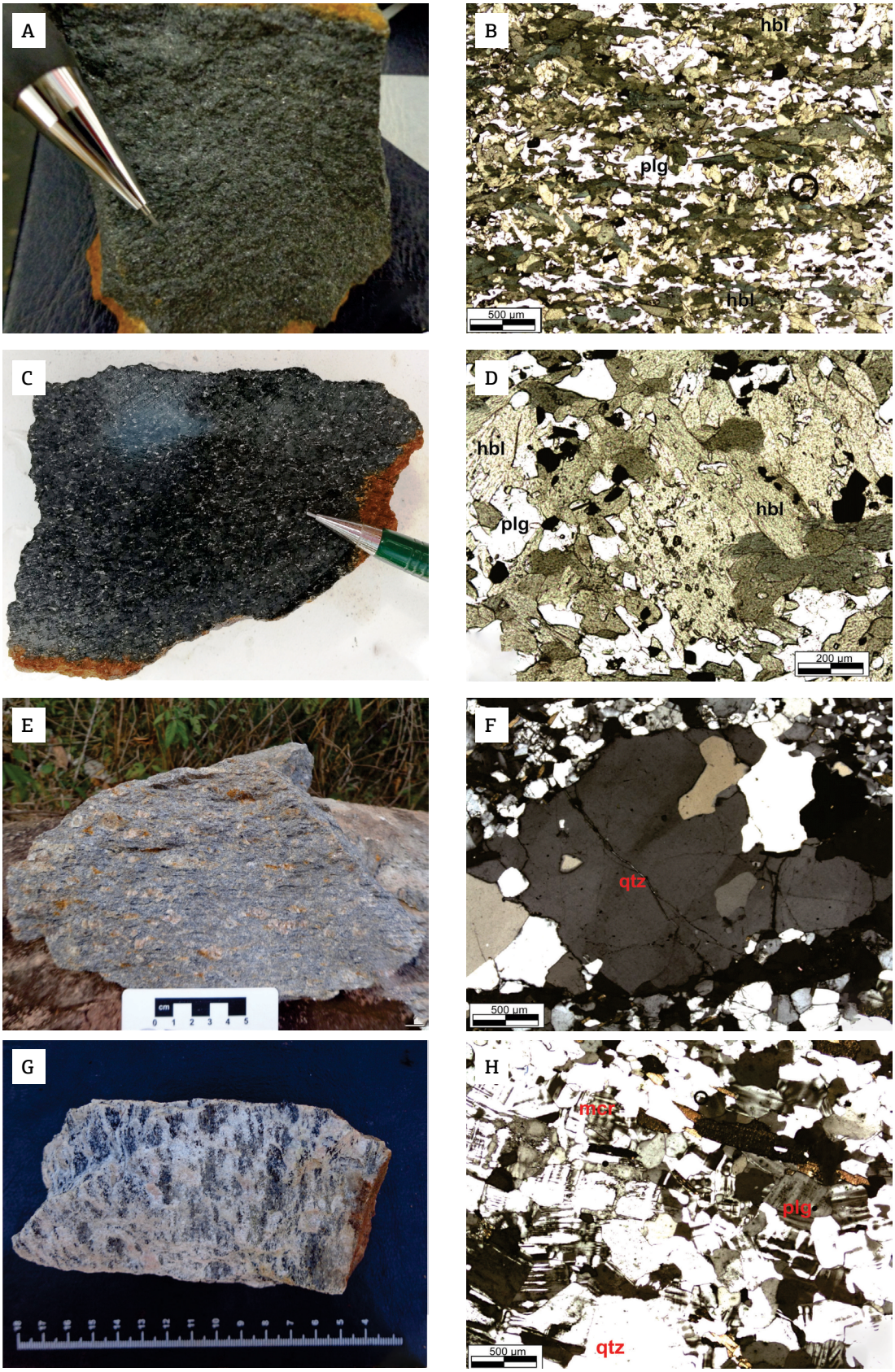

Figure 3. (A, B) fine-grained ortho-amphibolite samples composed essentially by hornblende, plagioclase, and quartz; (C, D) medium-grained ortho-amphibolite sample also characterized by hornblende, plagioclase and quartz; (E, F) quartz-feldspar porphyritic meta-rhyolite with a fine-grained matrix composed by microcline, quartz, plagioclase and biotite; (G, H) biotite granite coarse-grained.

Mg-hornblende to tschermakite, with higher Mg/(Mg+Fe^{2+}) ratios and silica contents in cores than borders, which in turn are richer in Al^{VI}, Al^{IV}, Fe, and Ti (Fig. 4A).

The plagioclase grains (up to 40% in volume) form granoblastic aggregates. Except one sample with low-Ca andesine (An_{31-44}) — they are non-zoned grains ranging from labradorite (An_{62}) to anorthite (An_{90}) (Fig. 4B). Quartz, accompanied or not by epidote, mostly forms fine-grained xenoblastic inclusions within plagioclase and amphibole, as exsolved silica excess. The chemical variations in amphibole (from Mg-hornblende to more Al-Fe rich types) and plagioclase (with increasing Ca contents) are consistent with growth under prograde metamorphism.

Felsic rocks

The meta-rhyolites are porphyroclastic rocks formed by a well-foliated fine-grained matrix of microcline, quartz, plagioclase and biotite, enveloping milimetric eye-shaped porphyroclasts of quartz and microcline (Fig. 3E and 3F). K-feldspar is the major mineral phase, containing mica and drop-like quartz inclusions, and ranging in composition between $Or_{93}Ab_{07}$ and $Or_{96}Ab_{04}$ (Fig. 4B). Quartz also forms symplectite intergrows with K-feldspar. Plagioclase crystals are oligoclase (An_{14-20}) in composition (Fig. 4B). They may show polysynthetic twinning, inclusions of quartz, mica and apatite, as well as saussurite. Brown biotite grains occur oriented according to the regional foliation and belong to the siderophyllite-annite series, showing a great variation in the Al^{IV} contents, as well as high values and small variation in Fe/(Fe+Mg) ratios varying from 0.859 to 0.876. Accessory phases are essentially zircon and apatite.

The meta-granitoids are foliated to isotropic, medium- to coarse-grained, biotite- and/or hornblende-bearing syenogranite to monzogranite (Fig. 3G). Feldspars may show drop quartz inclusions, and vermicular intergrowth with quartz. Saussuritization of plagioclase is a common process. Brown biotite occurs oriented according to the regional foliation or forming spotted aggregates. Accessory minerals include apatite, zircon, titanite, magnetite and, occasionally, garnet.

Whole-rock geochemistry

Mafic rocks

Results from major and trace elements analysis for 11 basaltic samples from the Alto Rio Guanhães suite are given in Supplementary Table A2. The concentrations of most major and trace elements, as well as high–field–strength elements (HFSE; *e.g.*, Nb, Zr, Y) and rare earth elements (REE), seem to represent the primary magmatic contents of the study samples. All samples have low LOI values (0.2 to 1.3 wt%).

The ortho-amphibolite is silica-oversaturated with normative quartz, hypersthene, albite and anorthite, which suggests that even after the crystallization of mafic minerals and feldspar there was still silica crystallizing as quartz. These samples are tholeiitic subalkaline basalts, with silica and alkali contents ranging from 45.1 to 49.3 wt% and 1.1 to 2.5 wt%, respectively. MgO values show a narrow variation ranging from 6.1 to 8.6 wt% with Mg# between 43.7 and 54.9.

The mafic rocks in the Alto Rio Guanhães region are characterized by moderate contents of Al_2O_3 (13.35–15.63%), $Fe_2O_{3(t)}$ (12.29–15.94%) and CaO (10.07–11.51%), and low P_2O_5 (0.18–0.40%). These rocks show moderate to high TiO_2 (1.83–2.80%) values. Compatible trace elements like

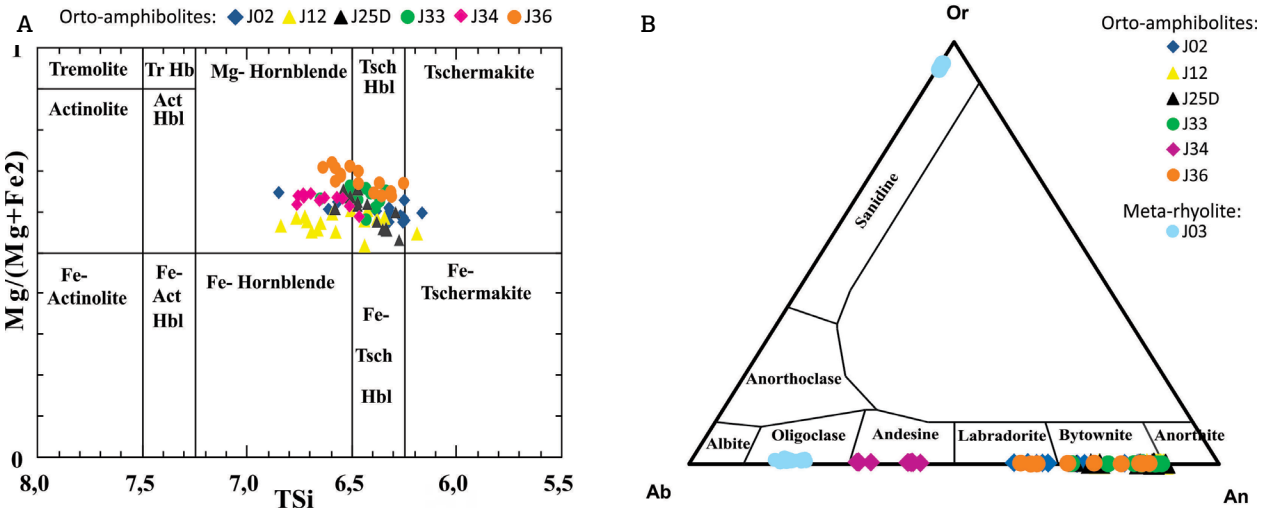

Figure 4. Chemical classification of the (A) amphiboles (after Leake *et al.* 1997) and (B) feldspars from the ortho-amphibolite and meta-rhyolite samples.

Ni and Cr correlate positively with the MgO contents. Ni ranges from 55 to 122 ppm and Cr from 75 to 233 ppm. The samples also display positive correlations of Mg# versus CaO and Al_2O_3, while opposite trends are given by TiO_2, $Fe_2O_{3(t)}$, MnO, P_2O_5, Zr, V, Nb, Y, Hf and REE.

The primitive-mantle-normalized spider diagrams (Fig. 5A) show depletions in Rb, Ba, K and Sr, while the chondrite-normalized REE patterns show an enrichment in light rare earth elements (LREE) with a La/Yb_N ratio ranging between 4.2 to 6.4 (Fig. 5B).

Felsic rocks

Major and trace element geochemical data of 53 felsic rock samples between meta-rhyolites and meta-granites are presented in Supplementary Table A2. Among these data, one analysis is from a meta-rhyolite collected for this study, while the remaining data have been compiled from the literature (Chemale Jr. 1987, Soares Filho 1987, Grossi Sad *et al.* 1990, Dussin 1994, Fernandes *et al.* 1994, Knauer and Grossi-Sad 1997, Oliveira 2002, Silveira-Braga 2012).

Similar to the ortho-amphibolites, the felsic rocks have sub-alkaline nature. The felsic volcanism is characterized by rhyolites while the plutonic rocks are mainly granites. The meta-rhyolites have high contents of SiO2 (66.94–78.60%) and low contents of MgO (0.08–0.76%), $Fe_2O_{3(t)}$ (0.92–7.43%), CaO (0.24–1.78%), TiO_2 (0.13–0.68%) and K2O (4.0–5.5%), with wide Al_2O_3 ranges (10.5–13.86%). They have total alkalis (Na_2O + K_2O) varying between 6.13 and 8.84%. These rocks are weakly metaluminous to peraluminous with A/CNK values 0.85–1.2 (Fig. 6A). The meta-rhyolites in the peraluminous fields may suggest contamination with supracrustal metasedimentary rocks.

The meta-granite samples show good geochemical correlations with the felsic volcanic rocks. They show high SiO_2 contents (67.80–78.63%) and low contents of MgO (0.01–0.54%), CaO (0.16–2.10%), K2O (3.7–6.7%) and $Fe_2O_{3(t)}$ (1.04–7.79%), with wide ranges of Al_2O_3 (10.4–13.8%) and alkalis (6.09–11.09%). They are metaluminous to weakly peraluminous and some samples plot in the alkaline field, with A/CNK values ranging between 0.7 and 1.2, and A/NK > 0.85 (Fig. 6A). They have high $FeO_{(t)}/(FeO_{(t)}$ + MgO)

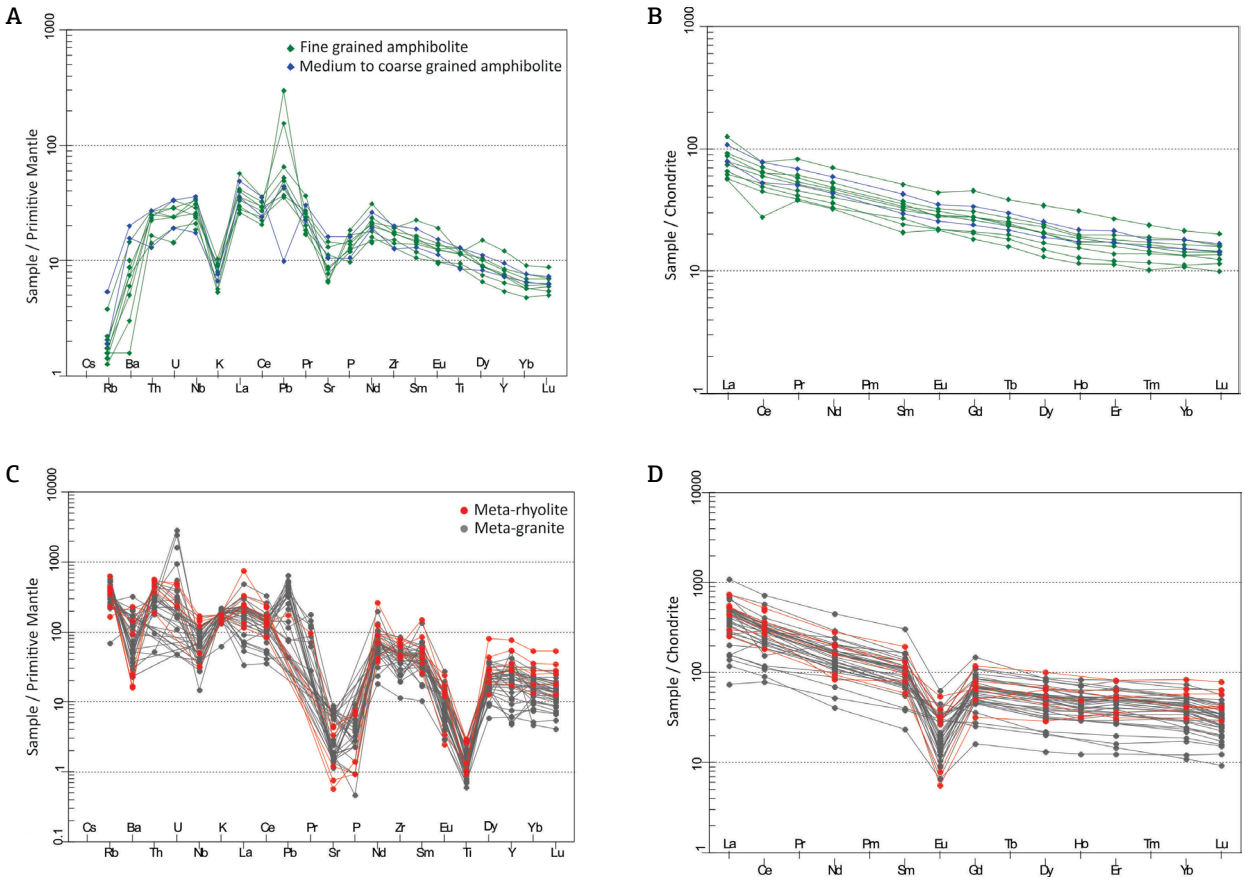

Figure 5. Primitive mantle and chondrite-normalized element spidergrams for: (A, B) mafic rocks and (C, D) felsic rocks from the Guanhães block. The normalization values are from Sun and McDonough (1989). For the meta-granites and meta-rhyolites, besides this work, data were compiled from Chemale Jr. (1987), Soares-Filho (1987), Grossi Sad *et al.* (1990), Dussin (1994), Fernandes *et al.* (1994), Knauer and Grossi-Sad (1997), Oliveira (2002) and Silveira-Braga (2012).

ratios and are further classified as ferroan alkali-calcic and ferroan calc-alkalic granites (Fig. 6B and 6C).

In general, the felsic rocks show remarkable depletion in Ba, Sr, P and Ti, suggesting plagioclase+apatite+Fe-Ti oxide fractionation (Fig. 5C and 5D). These rocks are slightly enriched in LREE, showing generally flat HREE patterns with large variations in $(La/Lu)_N$ ratios (3.41–24.40), $(La/Sm)_N$ ratios (1.91–5.15), $(Sm/Lu)_N$ ratios (0.92–6.83), and variable Eu anomalies (Eu/Eu* = 0.03–1.13).

Magmatic zircon data

Zircon U–Pb isotopic ages

An ortho-amphibolite (sample J02) and a meta-rhyolite (sample J03), both interlayered with metasedimentary rocks in the Alto Rio Guanhães unit, were selected for LA-ICPMS U–Pb, Lu-Hf and $\delta^{18}O$ isotope and REE in zircon analysis. Representative CL images of zircons from these volcanic rocks are shown in Fig. 7, along with the locations of spots measured for the in situ isotopic analyses.

Ortho-amphibolite

Zircons of the ortho-amphibolite are subhedral and irregularly shaped grains with average lengths of 100–200 μm and length to width ratios around 2:1. The oscillatory concentric zoning is typical of magmatic origin (Fig. 7). They have moderate U content with variable Th/U (0.06–1.24) (Suppl. Data A3). Thirty one spot data (from a total of 63) provide a robust Concordia age of 1725.1 ± 3.9 Ma (MSWD = 0.025; Fig. 8A), which is interpreted to represent the crystallization age of the igneous protolith.

Meta-rhyolite

The meta-rhyolite shows mostly euhedral, long prismatic zircon crystals with average lengths of 200–300 μm, length to width ratios mostly 3:1 and oscillatory magmatic zoning (Fig. 7). They show moderate U content with variable Th/U (0.42–1.42) (Suppl. Data A3). Sixty two data, from a total of 81 spots, also yield a robust Concordia age of 1747.8 ± 3.2 Ma (MSWD = 0.50; Fig. 8B), which constrains the crystallization age of the rhyolite.

Meta-granite

Zircons from a hornblende-biotite syenogranite (Açucena pluton) of the Borrachudos suite were dated using the SHRIMP technique. The grains are homogeneous with medium luminescence in CL image and show oscillatory zoning. The analytical results of 12 spots in 10 crystals are shown in Supplementary Table A3 and Fig. 8C. Eight spots belonging to the same population of crystals (MSWD = 0.69) yield a concordant grouping of 1740.5 ± 7.8 Ma, interpreted as the age of magmatic crystallization. Similar age is obtained by the 12 spots that define an upper intercept age of 1739.0 ± 8.8 Ma (MSWD = 0.73).

Hf isotope composition of zircons

Ten Hf isotopic spots analyses were conducted on zircons from the ortho-amphibolite (J02) and 12 analyses on those from the meta-rhyolite (J03). Analytical data are given in the Supplementary Table A4 and presented in Fig. 9A.

The zircons from the ortho-amphibolite show relatively uniform Hf isotopic compositions with radiogenic $^{176}Hf/^{177}Hf$ ratios of 0.281453 to 0.281571 for ages between 1717 and 1732 Ma. All analyzed zircon grains yielded consistently negative $\varepsilon Hf_{(t),}$ varying from -8.25 to -4.05, which suggests contamination during ascent through the crust. $^{176}Hf/^{177}Hf$ ratios for the analyzed spots of the meta-rhyolite zircons range from 0.28118 to 0.28132 with correspondent $\varepsilon Hf_{(t),}$ varying from -17.58 to -12.32 for ages between 1735 Ma and 1760 Ma, which suggests that this magma was essentially sourced from long-lived crustal rocks. The Hf (T_{DM}) model ages for the

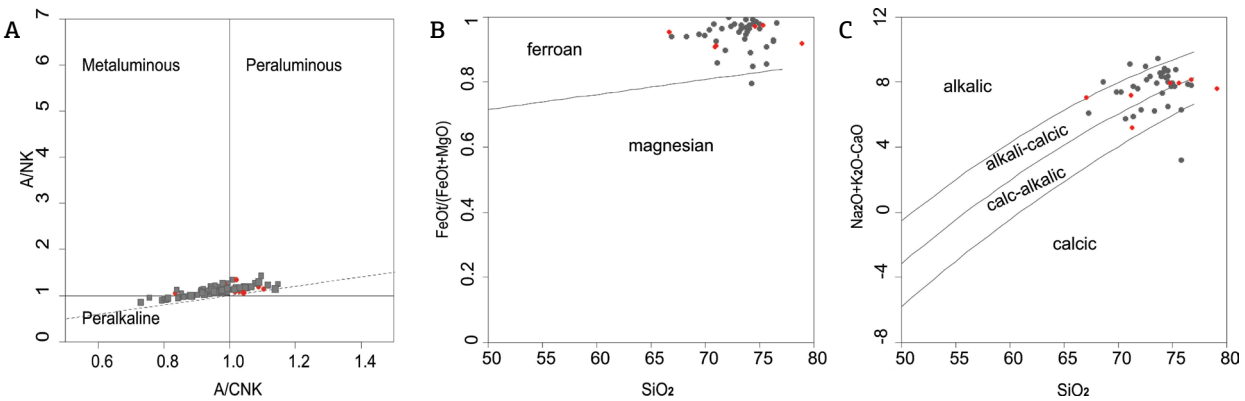

Figure 6. Granite tectonic discrimination diagrams for the felsic magmatism: (A) A/CNK vs. A/NK diagram (Shand 1943); (B) SiO_2 vs. FeOt/(FeOt + MgO) and (C) SiO_2 vs. $Na_2O + K_2O$-CaO from Frost et al. (2001). Additional data from Chemale Jr. (1987), Soares-Filho (1987), Grossi Sad *et al.* (1990), Dussin (1994), Fernandes *et al.* (1994), Knauer and Grossi-Sad (1997), Oliveira (2002) and Silveira-Braga (2012).

ortho-amphibolite zircon grains range between 2.28 Ga and 2.44 Ga, while those for the meta-rhyolite vary from 2.62 Ga to 2.80 Ga, indicating the involvement of Archean and possibly Siderian to Orosirian rocks in magma genesis.

Zircon O isotopes

The oxygen isotopic compositions of zircon grains from the ortho-amphibolite and meta-rhyolite samples are listed in Supplementary Table A4. There are no consistent differences in $\delta^{18}O$ between the rims and the cores of the analyzed grains in both samples.

The meta-rhyolite zircons have $\delta^{18}O$ values varying from 6.8 to 8.0, with 53% of the analyzed zircons (n = 27) showing values between 7.5 and 8.0 (Fig. 9B). For the ortho-amphibolite zircons, $\delta^{18}O$ values are variable from 5.6 to 7.9 (Fig. 9B), with 52% of the analyses between 7.0 and 7.5 (n = 16). Two grains have values around 5.6, which are similar to those of zircon crystallizing from uncontaminated mantle-derived magma (5.3 ± 0.3‰, Valley *et al.* 1998, Valley 2003).

The meta-rhyolite zircons show a $\delta^{18}O$ range typical of felsic rocks while the ortho-amphibolite zircon grains are consistent with contamination of mantle-derived magma that interacted with continental crust material (Valley *et al.* 2005, Bindeman 2008).

Trace element chemistry of zircons

Zircon grains from the ortho-amphibolite and meta-rhyolite have been analyzed for trace elements concentrations by LA-ICPMS. The measurements were performed in the zircon cores, in the same textural domains as the U-Pb and Lu-Hf analyses (Suppl. Data A4).

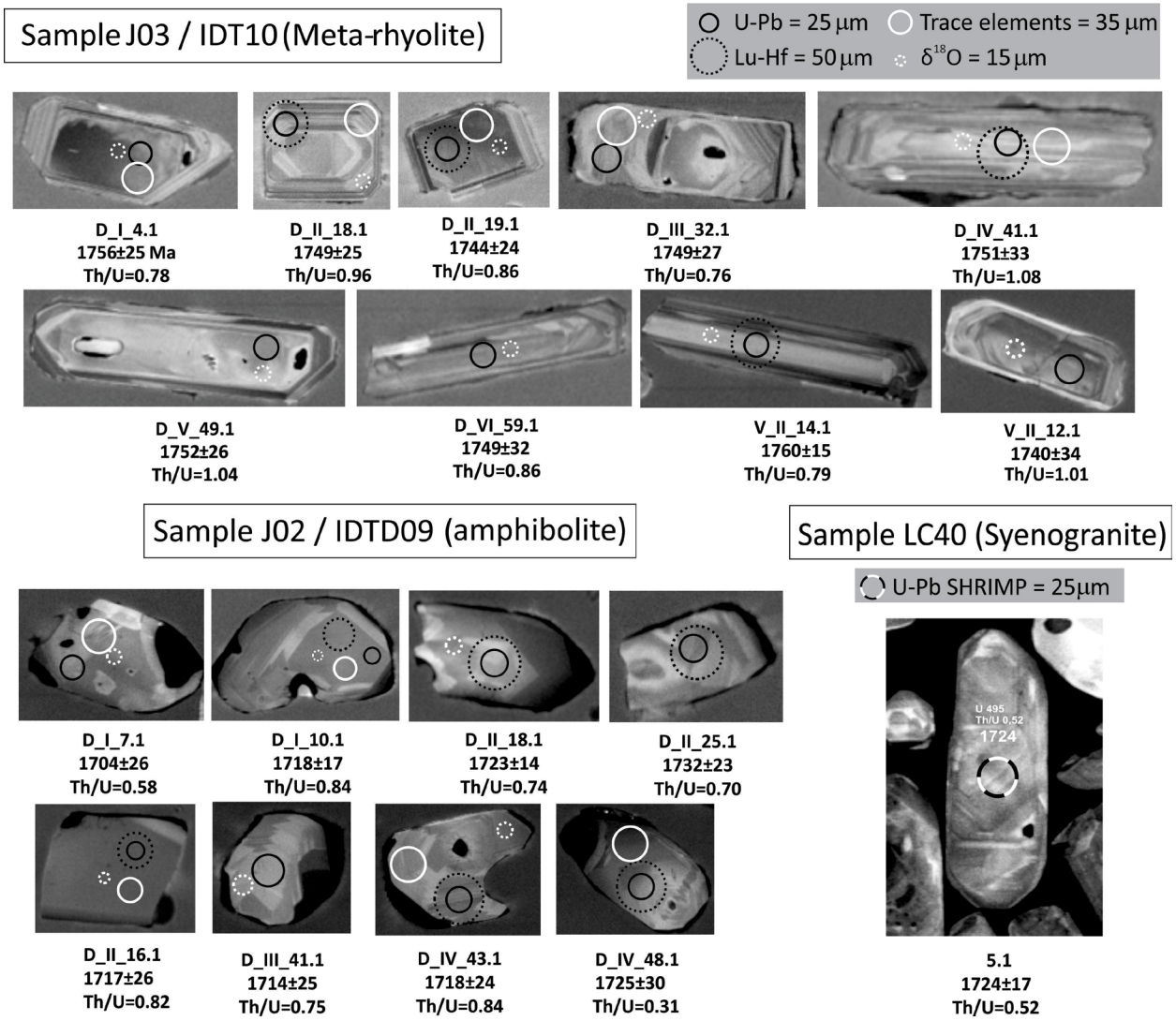

Figure 7. Representative cathodo-luminescence (CL) images for the zircons from the ortho-amphibolite sample J02, the meta-rhyolite sample J03 and the granitic sample LC-40, showing the location and the diameter of the spots for U-Pb, Lu-Hf and oxygen isotopes, and also rare earth elements (REE) analyses.

The grains of both samples show very similar REE patterns, with HREE enrichment and LREE depletion relative to chondrite values (Fig. 10A and 10B). The ortho-amphibolite zircons $(Sm/La)_N$ range from 48 to 431, $(Lu/Gd)_N$ values ranging between 11 to 24 and Th/U ratio from 0.3 to 0.8. The meta-rhyolite zircon grains display $(Lu/Gd)_N$ values between 11 to 19, and the Th/U ratio varies from 0.7 to 1. The REE patterns show positive Ce anomaly and negative Eu anomaly, features consistent with unaltered igneous zircon (Hoskin and Schaltegger 2003, Rubatto 2017). The negative Eu anomaly is typical of plagioclase fractionation while the positive Ce anomaly is related to oxidation processes or to an oxidizing environment (Hoskin and Schaltegger 2003).

The REE patterns are similar to populations of crustal zircon (Hoskin and Schaltegger 2003, Grimes *et al.* 2007, Harley and Kelly 2007) and overlap the REE concentration of zircons from oceanic crust and continental granitoids (Fig. 10A and 10B). This correspondence between the REE concentration of zircons from different types of rocks can be explained by the REE compatibility in the zircon lattice (*e.g.*, Grimes *et al.* 2007).

The zircon crystals from both samples have intermediate U/Yb ratio. The Hf and Y vs. U/Yb discriminant diagrams attest the continental nature for the meta-rhyolite zircon grains and indicate crustal input for the ortho-amphibolite zircons (Fig. 10C and 10D).

DISCUSSION

Here we discuss the petrogenesis of the mafic and felsic magmatism related to the Espinhaço rift system, the correlations in view of the Statherian scenario in the São Francisco block, as well as the global inferences in relation to paleo-continental settings.

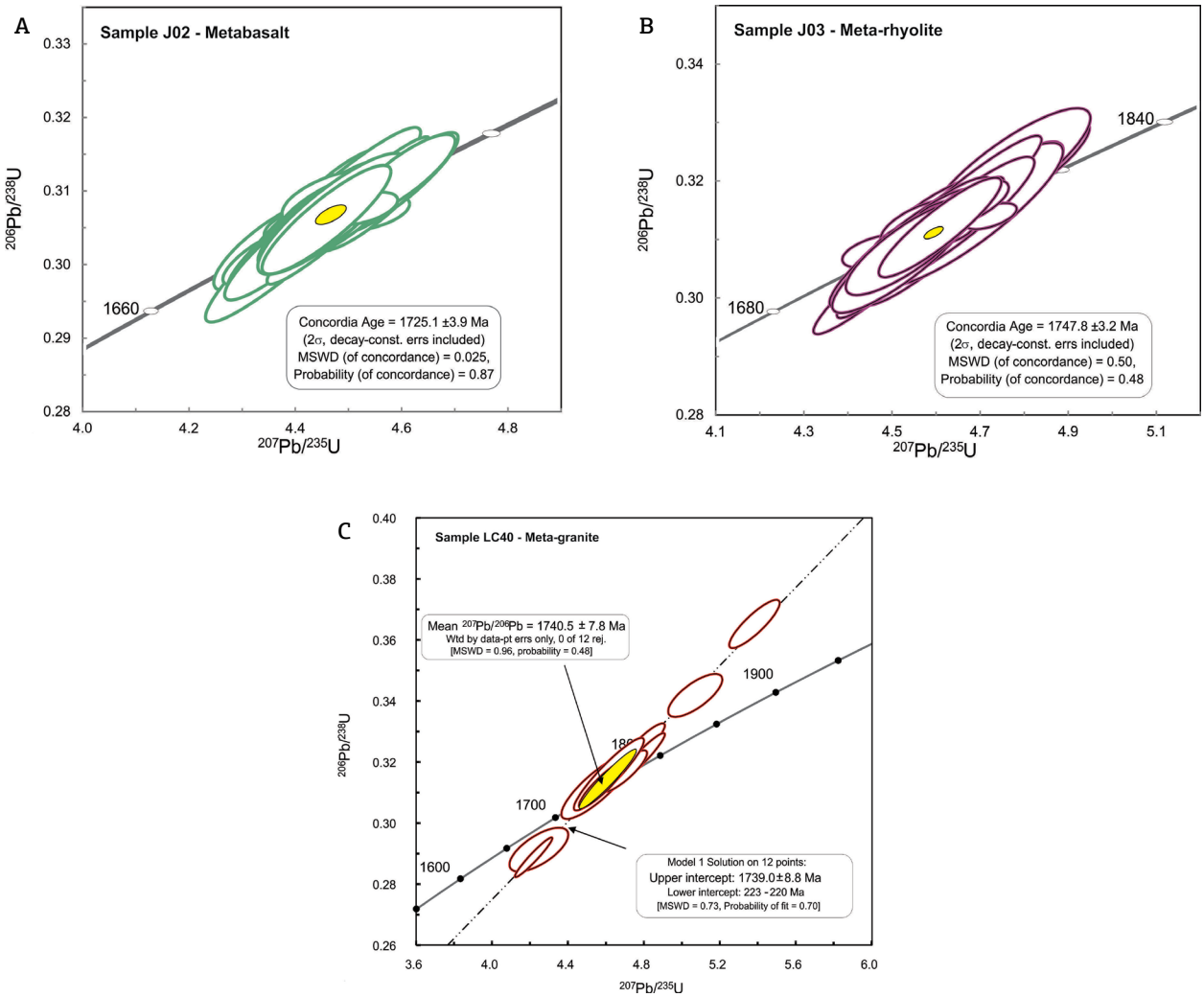

Figure 8. LA-ICPMS zircon U–Pb concordia diagrams of samples: (A) J02 — ortho-amphibolite, (B) J03 — meta-rhyolite, (C) LC40 — biotite granite.

Petrogenesis

Petrogenesis of the mafic rocks

Magmatic crystallization

The mafic rocks from the Alto Rio Guanhães unit have compositions suggesting that fractional crystallization played an important role in the petrogenesis of the basaltic magmatism. These rocks are characterized by positive correlation of CaO, Na_2O, Al_2O_3, Ni and Cr, in relation to Mg#, suggesting fractionation of olivine, pyroxene and plagioclase. The negative Sr anomaly of most samples corroborates plagioclase fractionation. The range between the ratios of the incompatible trace elements (Zr, Y, Nb) of the distinctly

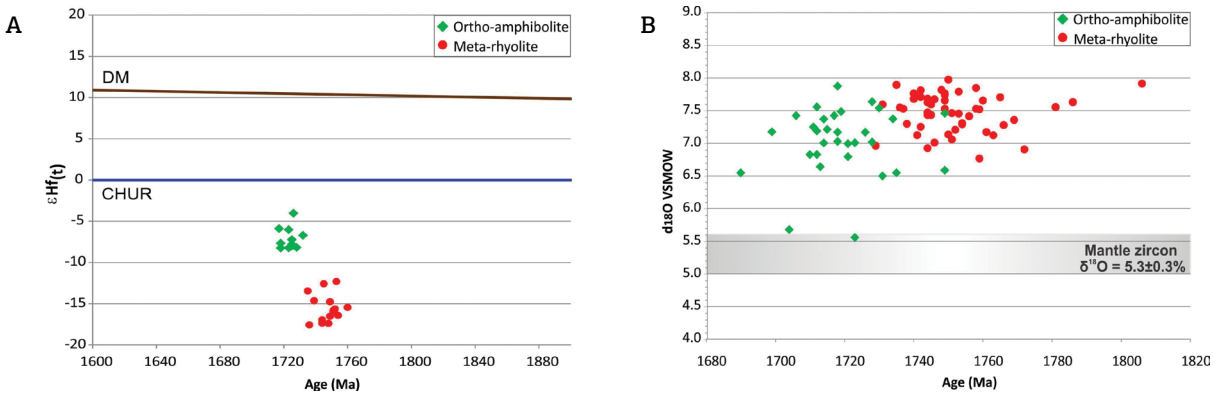

Figure 9. Schematic diagrams for Lu-Hf isotopic evolution vs. U-Pb age (A) and for $\delta^{18}O$ isotopic evolution vs. U-Pb age (B) for zircons from ortho-amphibolite and meta-rhyolite samples. The values of mantle zircons are from Valley *et al.* (1998) and Valley (2003).

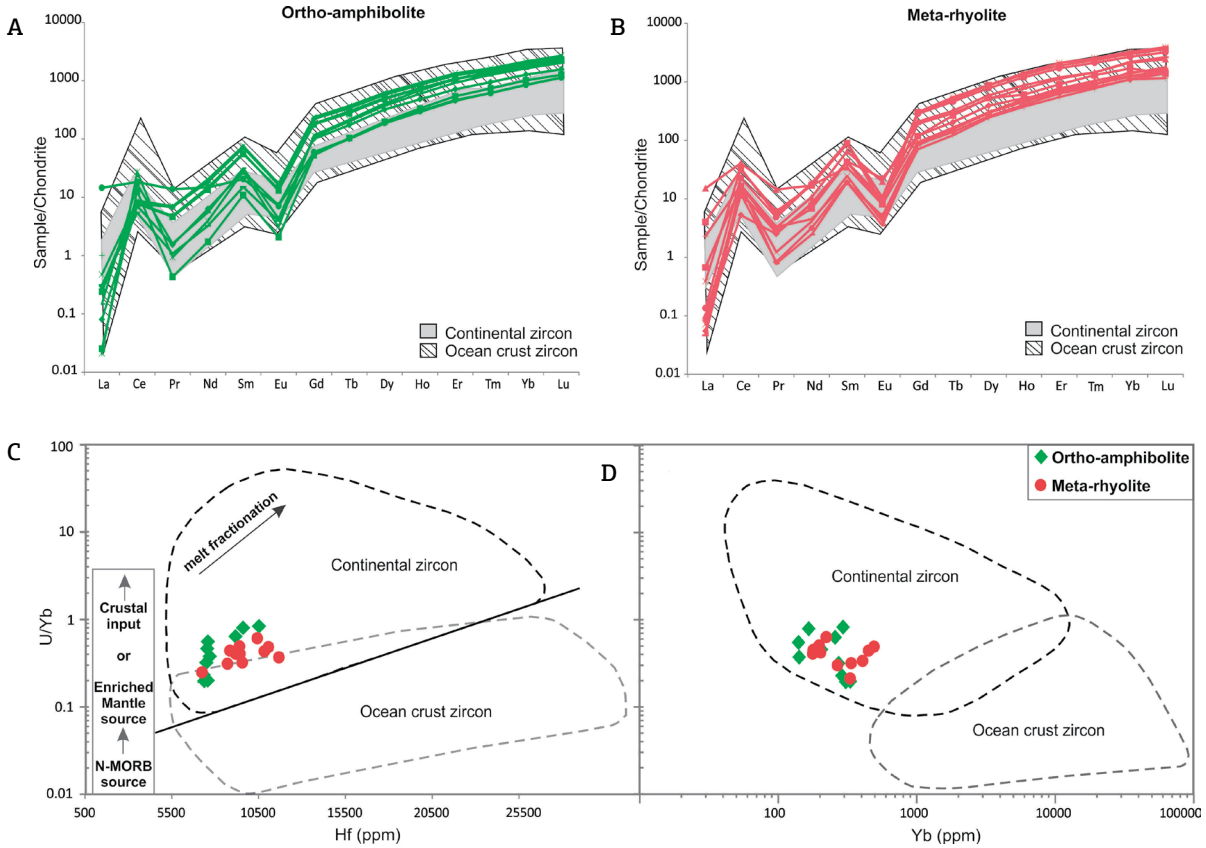

Figure 10. Representative rare earth elements (REE) patterns of zircon grains determined by in situ analysis (LA-ICP-MS) for the ortho-amphibolite (A) and meta-rhyolite (B) normalized to chondrite (McDonough and Sun 1995). Plots (C) and (D) show geochemical discriminant diagrams with continental and ocean crust zircon fields. The values of continental and ocean crust zircons are from Grimes *et al.* (2007).

evolved samples is less than 12%. This and the absence of compositional gaps and the Pearson correlation coefficient values suggest that fractional crystallization process was involved in the generation of these rocks.

Considering that the ratios of incompatible elements that have similar geochemical behavior tend to remain constant during fractional crystallization, the plot in the Figure 11A shows the decreasing values of Ni accompanied by constancy of Zr/Nb ratio.

Assimilation and fractional crystallization (AFC)

In general, fractional crystallization is accompanied by assimilation of crustal material, mainly in rift-related environments. The negative values of $\varepsilon Hf_{(t)}$ in zircons between -4.05 to -8.25 for the ortho-amphibolite sample indicate a moderately juvenile magma significantly contaminated by continental crust material. The $\delta^{18}O$ data registered for these zircon grains characterizes shifted magmatic $\delta^{18}O$ values by crustal assimilation (item 3.3.3). Crustal input is also suggested by the U/Yb ratio of zircons (item 3.3.4).

Thus, in order to evaluate the influence of crustal contamination during the mafic magma ascent and/or residence in magma chamber, the DePaolo (1981) equation was used to verify the involvement of AFC processes. The results presented in Fig. 11B show that the values of Zr and Nb incompatible trace elements of the mafic samples, among others, can be explained by up to 30% of AFC process in the upper crust.

Magma mantle source

On the basis of the above discussion (items 4.1.1.1 and 4.1.1.2), fractional crystallization and crustal assimilation

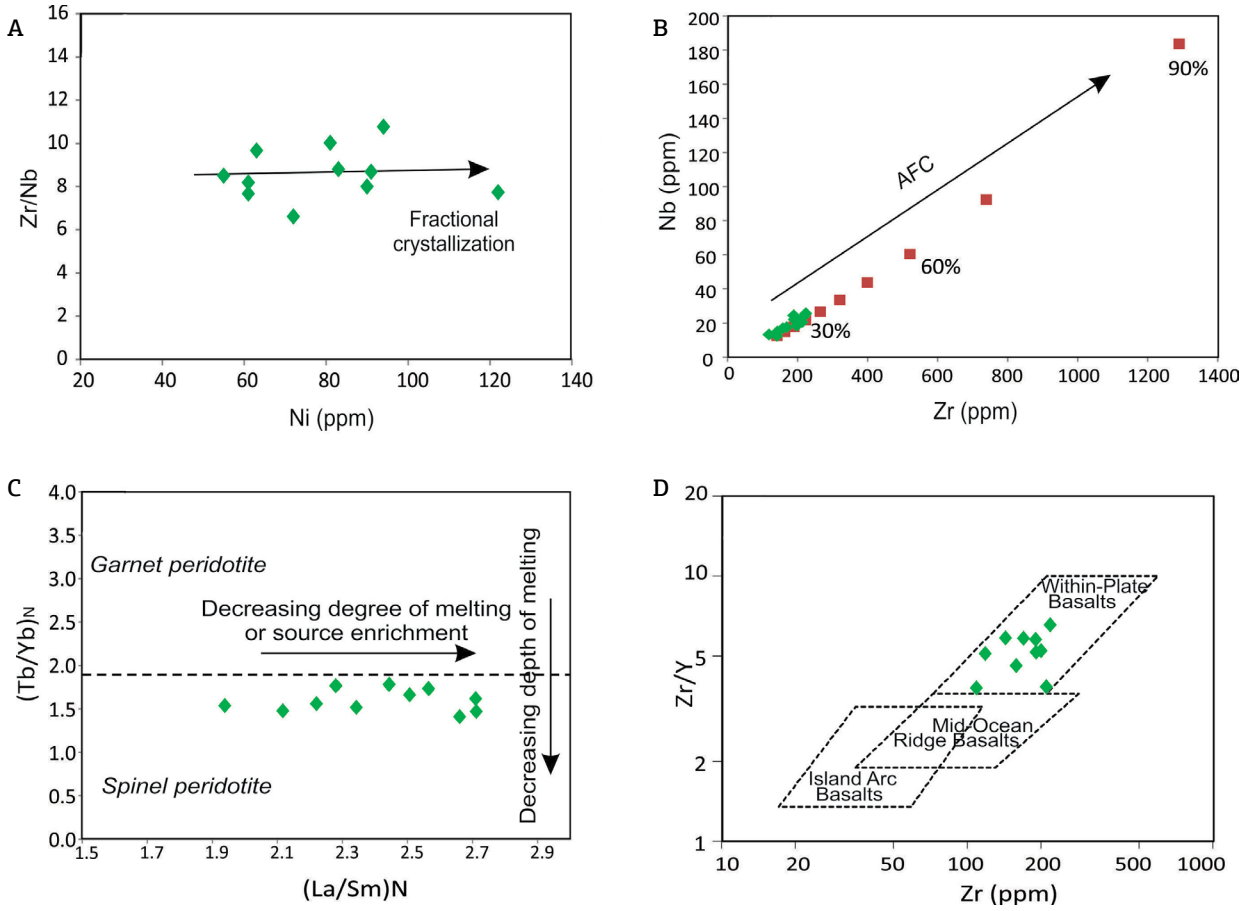

Figure 11. Trace element variation diagrams for the Alto Rio Guanhães mafic suite. (A) Ni vs. Zr/Nb. (B) Assimilation and fractional crystallization (AFC) model for Zr vc Nb. The AFC curve (red squares) shows ranges of 10% (between 0 and 90%). The arrow indicates that the tendency of the magmatic evolution of the analyzed mafic rocks (green diamond) is the same of the AFC curve, indicating values up to 30% AFC. The continental crust chemical data is from Taylor and McLennan (1985), and the mineral/melt partition coefficients for basaltic liquids are after the compilation of Rollinson (1993). (C) $(La/Sm)_N$ vs. (Tb/Yb) diagram to determine the source of the mafic magmas. The horizontal dashed line separates the fields for melting of garnet-bearing peridotite and of spinel-bearing peridotite Wang *et al.* (2002). Normalization values of the chondrite C1 after Sun and McDonough (1989). (D) Zr vs. Zr/Y discrimination plot (Pearce and Norry 1979).

were important processes in the petrogenesis of the mafic magmatism in the Alto Guanhães unit. The similar REE and trace element patterns for theses rocks (Fig. 5A and 5B) suggest a common mantle source for them.

The amount of melting required to generate tholeiitic basaltic melts from the peridotitic mantle ranges from 10 to 20% (Jaques and Green 1980). Owing to the distinctive REE partition coefficients between garnet and spinel during melting of spinel peridotites vs. garnet peridotites, a spinel-bearing peridotite source is suggested for these rocks (Fig. 11C). The Alto Rio Guanhães mafic suite is characterized by low $(Tb/Yb)_N$ ratios (1.4–1.8) and $(Gd/Yb)_N$ ratios (≤ 2), typical of rocks generated by partial melting of a mantle source in the spinel-stable field and, thus, at depths less than 60–70 km (Wilson 2007). The magmatism shows variation of degrees of melting or source enrichment, according to the $(La/Sm)_N$ range (1.9–2.7). The limited range of $(Tb/Yb)_N$ ratios also suggests small variation in the depth of melting, relating to small variation in the crustal thickness during the progressive continental rifting.

La/Yb and La/Nb ratios can be used as indicative for discriminating fertile, enriched and depleted mantle sources. The meta-mafic rocks show $(La/Yb)_N > 1$ (4.0–6.5) and $(La/Nb)_N > 1$ (1.2–2.2) that are characteristics of an enriched source associated with the lithospheric mantle (Sun 1980, Humphris *et al.* 1985, Sun and McDonough 1989), as expected in continental rift systems. Despite the range of the major and trace elements, the meta-mafic samples from the Alto Rio Guanhães unit generally exhibit incompatible trace elements patterns more enriched than E-MORB, except for the values of Rb, Ba and Sr, which resemble N-MORB (Fig. 12). However, such signatures may be expected for evolved continental rift systems.

Tectonic setting

The mafic rocks of the Alto Rio Guanhães unit have never been dated in detail, as well as all other rocks of the Espinhaço system. The studied mafic rocks show patterns of incompatible trace elements comparable to those of intraplate basalts, such as high Ti and Zr, instead of basalts of volcanic arc and meso-oceanic ridge. Regarding the Pearce and Norry (1979) (Fig. 11D) and Wood (1980) diagrams, widely used for basaltic rock discrimination, all samples plot in the intraplate basaltic field, suggesting that the Alto Rio Guanhães mafic magmatism occurred in an attenuated continental lithosphere. Furthermore, the age of this magmatism fits very well with the age range of the felsic rocks found throughout the Espinhaço system. Thereby, this mafic magmatism can be related to the same continental taphrogenic process that developed during the Statherian in the São Francisco paleocontinental region.

Petrogenesis of the felsic rocks

Chemical proxies for anorogenic magmatism

The meta-rhyolites and intrusive granites in the Guanhães block show negative correlations between SiO_2 and TiO_2, $FeO_{(t)}$, CaO and Al_2O_3, suggesting fractionation of hornblende, biotite and Fe-Ti oxides during magma evolution. CaO and Al_2O_3 contents coupled with compatible behavior of Sr, Eu and Ba with SiO_2, point to fractionation of plagioclase. In the plots Sr vs. Rb (Fig. 13A), the variations in these contents seem to be mainly related to fractionation of plagioclase and K-feldspar.

The compatible/incompatible element ratios, such as Rb/Sr and K/Rb, are used to recognize the degree of fractionation of granitic magmas (*e.g.*, Blevin 2003). In the SiO_2 vs.

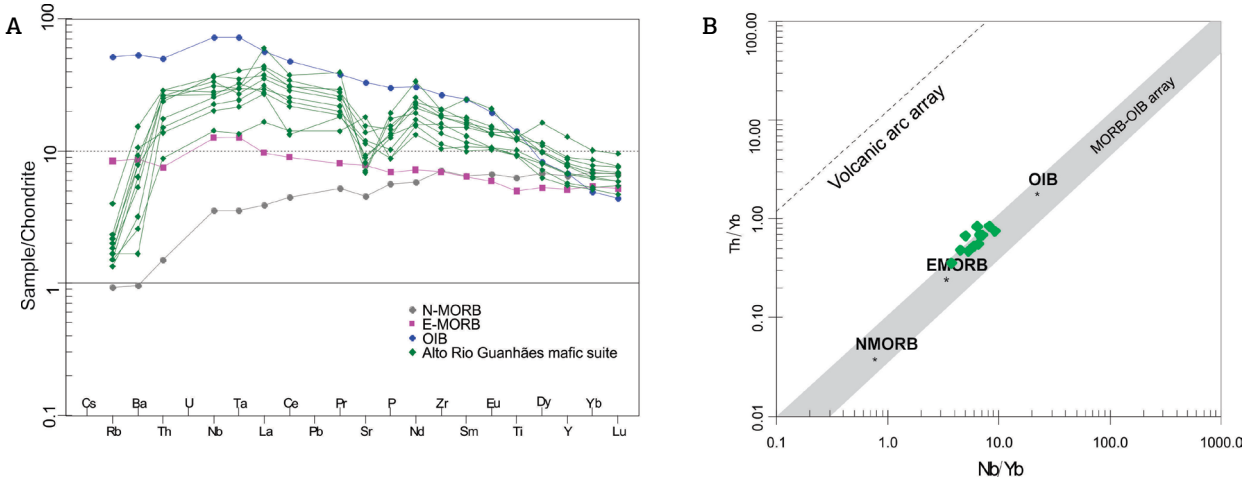

Figure 12. (A) Comparison of primitive mantle-normalized incompatible trace element spidergrams for the amphibolites of the Alto Rio Guanhães suite, with that of oceanic island basalts (OIB), E-type and N-type MORBs. Patterns for OIB, E-MORB and N-MORB are from Sun and McDonough (1989). (B) Nb/Yb vs. Th/Yb discrimination diagram from Pearce (2008).

K/Rb and SiO_2 vs. Rb/Sr diagrams (Fig. 13B and 13C), the granitic rock compositions in the study area plot in the moderately and strongly evolved fields, showing characteristics of differentiated magmas. This suggests an evolution for the granitic compositions by fractional crystallization processes.

These felsic rocks have high SiO_2 and alkali contents, and are generally enriched in HFSE and REE. The Ga/Al*1000 ratios range from 2.8 to 7.5, which is typical of A-type granites, according to Whalen *et al.* (1987). These felsic magmatism also fits in the definition of A-type granitic rocks by Loiselle and Wones (1979) since they present, in addition to SiO_2 and alkalis, high levels of Nb, Zr, REE, negative Eu anomaly and low values of CaO and MgO. According to the geochemical subdivision of A-type granites proposed by Eby (1992), this felsic magmatism belongs to sub-type A2 (Fig. 13D).

Tectonic setting and magmatic evolution

A-type felsic magmas are usually generated in extension environments, where crustal stretching, mantle uplift and the heat transferred from the mantle can reach the shallowest levels of the crust (Loiselle and Wones 1979). However, the origin of A-type magmatism is quite controversial and the mechanics available in the literature describes both melting process of continental crust by underplating of melts derived from the mantle, and an evolution by fractional crystallization of basaltic magmas concomitant with crustal assimilation — AFC (*e.g.*, Whalen *et al.* 1987, Eby 1992, Rollinson 1993, Peccerillo *et al.* 2003).

The studied meta-rhyolites and intrusive granites do not present evidence of being products of evolutionary processes involving mafic magmatism. The volume of felsic rocks is much larger than the mafic rocks and can not be explained by fractional crystallization processes of basaltic magmas. The surface area covered only by the Borrachudos granites is bigger than 6.000 km^2. In addition, the felsic rocks show high ratios between incompatible trace elements, as Th/La, Zr/Ti and Th/Nb, in contrast to the values obtained for the mafic magmatism, which are up to 15 times smaller.

The felsic magmatism is characterized by highly negative values of $\varepsilon Hf_{(t)}$ (-12.32 to -17.58), indicating association with crustal material. The same is revealed by the positive $\delta^{18}O$ values (7.02 to 7.98) and REE pattern of these zircon grains. The Hf T_{DM} ages argue against a simple magmatic differentiation model, suggesting the generation of felsic magmas from an ancient continental crust. In the tectonic classification diagrams from Pearce *et al.* (1984), the samples plot in the field of intraplate granites (Fig. 13E and 13F).

The geochemical signature of the felsic bodies, both plutonic and volcanic, is very similar (item 3.2.2), indicating that they could be derived from fractionation of a crustal

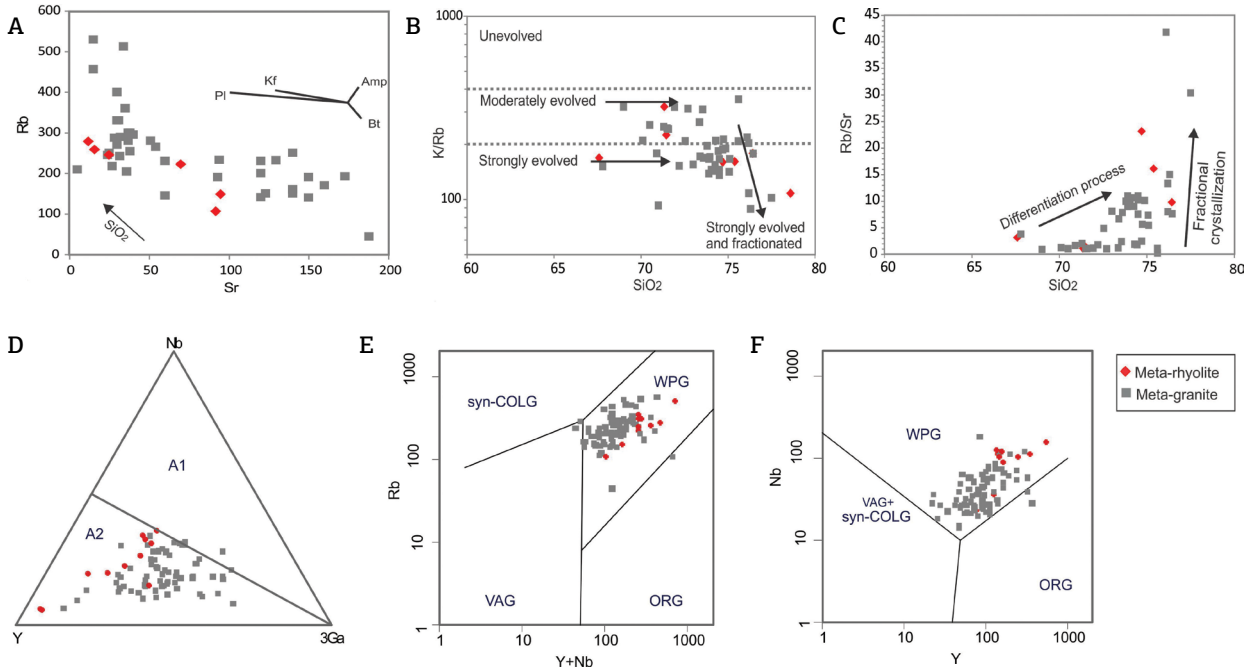

Figure 13. Trace element variation diagrams for the meta-granites and meta-rhyolites in the Guanhães block showing different fractional crystallization trends: (A) Sr vs. Rb; (B) SiO_2 vs. K/Rb; (C) SiO_2 vs. Rb-Sr. (D) Nb-Y-3Ga discrimination diagrams for the subdivision of the A-type granites by Eby (1992). (E) Y+Nb vs. Rb and (F) Y vs. Nb tectonic classification diagrams from Pearce *et al.* (1984). Additional data from Chemale Jr. (1987), Soares-Filho (1987), Grossi Sad *et al.* (1990), Dussin (1994), Fernandes *et al.* (1994), Knauer and Grossi-Sad (1997), Oliveira (2002) and Silveira-Braga (2012).

source. The data reveal that they were generated by partial melting of materials from an Archean lower crust.

Statherian geochronological framework of rift-related magmatism of the São Francisco block

The Supplementary Table A5 summarizes the U-Pb and Pb-Pb ages of magmatic events related to the Statherian Espinhaço rift system recorded in the Guanhães block, Espinhaço Ridge and Chapada Diamantina, and also in correlated areas in the São Francisco block. These magmatic events are related to taphrogenetic processes that marked the São Francisco-Congo paleocontinent during the Late Paleoproterozoic (*e.g.*, Dussin 1994, Danderfer *et al*. 2015, Cederberg *et al*. 2016, Dussin 2017).

The tholeiitic meta-mafic rocks of the Alto Rio Guanhães unit are the first detailed studied record of a Statherian mafic suite coexisting with the well-known felsic magmatism related to the Espinhaço rift system. The only geochronological record so far for a mafic rock in the Guanhães block was presented by Dussin *et al*. (2000), which yielded 1697 ± 10 Ma $^{207}Pb/^{206}Pb$ single zircon evaporation data as the crystallization age of an amphibolite intercalation on metasedimentary rocks from the Guanhães Group. In the Southern Espinhaço Range (Fig. 1), highly metamorphosed and altered meta-volcanic mafic rocks associated with the opening of the Espinhaço basin show ages between 1747 Ma and 1700 Ma (Dussin 1994, Chemale Jr. *et al*. 2012a, Bezerra-Neto 2016, Silva 2016).

The precise in situ U-Pb dating of a meta-mafic rock from the Guanhães block presented in this study (1725 ± 4 Ma) is somewhat higher than the previously reported age by Dussin *et al*. (2000), but is within the age range of the meta-volcanic mafic rocks of the Southern Espinhaço. More recently, a meta-volcanic mafic rock from the Central Espinhaço ridge domain yielded an age of 1730 ± 8 Ma (Moreira 2017), which is virtually the same age obtained for the ortho-amphibolite of the Alto Guanhães unit.

The 1748 ± 3 Ma age for the meta-rhyolite also constraints a deposition age for the sedimentary infill of the Alto Rio Guanhães basin and allows us to correlate it with the whole Statherian Espinhaço rift system. The age of the meta-rhyolite (1748 ± 3 Ma) of the Alto Rio Guanhães unit is somewhat older than the Conceição do Mato Dentro meta-rhyolite (1715 ± 5 Ma; Machado *et al*. 1989) of the Southern Espinhaço domain, which is one of the nearest occurrences of such rocks in relation to the study area. Except this case, the Alto Rio Guanhães meta-rhyolite age is very similar to the U-Pb ages obtained for most felsic volcanic and plutonic rocks found along the Espinhaço system, like the Planalto de Minas meta-rhyolite (1752 ± 2 Ma; Machado *et al*. 1989) and a volcaniclastic rock (1758 ± 18; Costa 2017), both of the Central Espinhaço domain; the Rio dos Remédios meta-rhyolites of the Chapada Diamantina domain (1748 ± 4 Ma and 1752 ± 4 Ma; Babinski *et al*. 1994, Schobbenhaus *et al*. 1994); the Sapiranga meta-volcanic rock (1740 ± 10 Ma; Danderfer *et al*. 2015) of the Northern Espinhaço domain; the Lagoa Real plutonic suite found between the Chapada Diamantina and Northern Espinhaço domains (1744 ± 2 Ma, Pimentel *et al*. 1994); and the here presented U-Pb SHRIMP age for the Borrachudos suite (1740 ± 8 Ma).

The metasedimentary rocks of the Statherian Espinhaço basin, as quartzites and meta-conglomerates, show maximum depositional ages between 1.80 and 1.68 Ga and are well exposed in all Espinhaço rift branches (Danderfer *et al*. 2009, Chemale Jr. *et al*. 2012a, Santos *et al*. 2013). In the eastern edge of the Southern Espinhaço ridge, near the Guanhães block, Rolim *et al*. (2016) found a maximum depositional age of ca. 1666 Ma for a quartzitic unit. The available geochronological data for the quartzites and banded iron formations of the Guanhães Group suggest a maximum deposition average age of ca. 2080 Ma, with a single Statherian zircon age of 1737 ± 19 Ma (Barrote 2016). For the southern region of the Guanhães block, Statherian depositional ages (ca. 1668 Ma) were obtained to a meta-siliciclastic succession with iron formation intercalations (Carvalho *et al*. 2014, Silveira-Braga *et al*. 2015).

The U-Pb dataset for the whole Espinhaço system shows a wide age variation between 1790–1700 Ma, but a concentration in the time interval of ca. 1750–1710 Ma. The lower part of the rift system is characterized by large volume of acid magmatism, whereas the mafic magmatism is only registered in the upper supracrustal successions of the Statherian Espinhaço system, as well as in the Guanhães block. Contrasting with the mafic magmatism so far restricted in space, both the plutonic and volcanic felsic rocks are found along the whole Espinhaço rift system.

Intracontinental magmatism of Statherian age is also recorded in the south and west regions of the São Francisco paleocontinental block. To the south, the Pará de Minas mafic dyke swarm (Chaves 2001, Cederberg *et al*. 2016), which shows two Statherian dyke generations (ca. 1795 Ma and 1710 Ma; Cederberg *et al*. 2016), can be correlated in space and time to the Espinhaço rift system. Along the São Francisco northwestern region, it is well-documented the Statherian (1771–1768 Ma) meta-rhyolites and related A-type plutonic rocks of the Araí rift system (Pimentel *et al*. 1991).

Tectonic implications and global inferences

Paleotectonic constrains for the São Francisco-Congo paleocontinent

The São Francisco and Congo paleocontinental blocks (Fig. 1A) amalgamated after an orogenic event that took place

in the Rhyacian — Orosirian boundary. Since then, they became part of a paleocontinent that was only broken up by the opening of the South Atlantic Ocean in the Cretaceous. From the Rhyacian — Orosirian to the Neoproterozoic Brasiliano — Pan-African orogenic events only taphrogenic records have been reported with solid data in the focused region of the São Francisco — Congo paleocontinental block (Noce *et al.* 2007b, Pedrosa-Soares *et al.* 2008, Pedrosa-Soares and Alkmim 2011, Heilbron *et al.* 2017).

Distinct paleotectonic and paleogeographical reconstructions have been envisaged for the São Francisco-Congo paleocontinental block in Paleoproterozoic time, since those focusing the agglutination of Atlantica (ca. 2 Ga; Rogers 1996) and Columbia (1.90–1.70 Ga; *e.g.*, Zhao *et al.* 2004, Hou *et al.* 2008, Cederberg *et al.* 2016) to the Central African block (Cordani *et al.* 2013, D'Agrella-Filho and Cordani 2017).

Based on geotectonic, geochronological and paleomagnetic evidence, D'Agrella-Filho and Cordani (2017) suggested that the São Francisco-Congo, Kalahari, Borborema, Trans-Sahara, Rio de la Plata and smaller paleocontinental blocks assembled in the Central African block around 2 Ga, a paleocontinent diachronic but independent to the Columbia supercontinent (Fig. 14A).

Alternatively, there are models picturing the São Francisco-Congo block within the Columbia supercontinent (*e.g.*, Rogers and Santosh 2002, Zhao *et al.* 2004, Hou *et al.* 2008, Teixeira *et al.* 2017). Hou *et al.* (2008) envisaged a continuous subduction-related magmatic belt bordering Columbia that was amalgamated by orogenic systems developed from ca. 2.1 Ga to ca. 1.8 Ga. (Fig. 14B). In this configuration, the São Francisco — Congo craton, located in the border of Columbia, is juxtaposed to the Amazonian craton, linking the South America to Columbia through the Trans-Amazonian orogen. After this model, Danderfer *et al.* (2015) related the evolution of the Espinhaço rift system to a far-field continental extension induced by orogenic processes located in the Amazonian domain.

Recent paleotectonic models quoting the Statherian anorogenic magmatism suggest a paleocontinental link between the São Francisco and North China cratons (Peng 2015, Cederberg *et al.* 2016, Teixeira *et al.* 2017; Xu *et al.* 2017). These authors point to similarities between the Pará de Minas dyke swarm, located in the southern tip of the São Francisco craton, and the magmatism related to the Xiong'er-Taihang LIP event, both interpreted as related to Statherian intracontinental setting (Fig. 14C).

In this framework, the magmatism related to the Espinhaço rift system, including the Alto Rio Guanhães mafic suite, can be correlated to the Pará de Minas mafic dyke swarm and, probably, to the Xiong'er-Taihang magmatism. This suggestion is supported by geochemical (*e.g.*, trace element patterns; Fig. 15) and geochronological data from the Pará de Minas mafic dyke swarm (Chaves 2001), the Xiong'er volcanic rocks (Zhao *et al.* 2002, Peng *et al.* 2008, He *et al.* 2009, Wang *et al.* 2010), the Taihang dykes (Hou *et al.* 2001, Peng *et al.* 2004, 2008, Peng 2015, Wang *et al.* 2004, 2007, 2008) and the tholeiitic amphibolites of the Alto Rio Guanhães mafic suite (this work).

The younger dyke generation of the Pará de Minas dyke swarm (1717–1702 Ma; Cederberg *et al.* 2016) can be chrono-correlated to the metamorphosed volcanic and

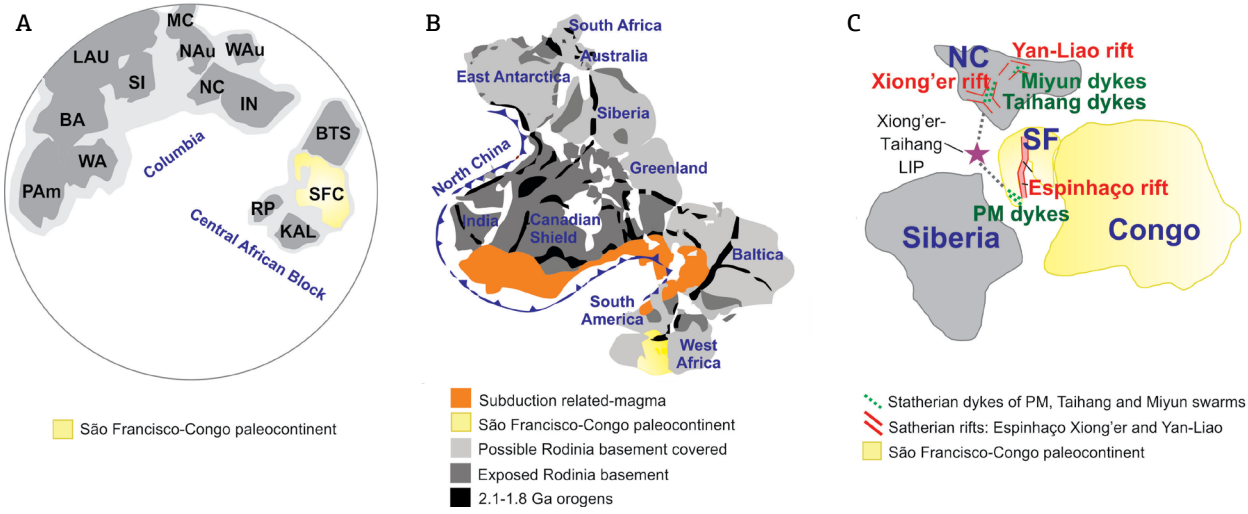

Figure 14. Paleogeographic reconstruction models involving the paleocontinent São Francisco-Congo in the context of Columbia at 1.78 Ga: (A) D'Agrella-Filho and Cordani (2017); (B) Hou *et al.* (2008); (C) Cederberg *et al.* (2016). Laurentia (LAU), Baltica (BA), Proto-Amazonia (PAm), West Africa (WA), Siberia (SI), Mawson continent (MC—South Australia plus East Antarctica), North Australia (NAu), West Australia (WAu), North China (NC), India (IN), Rio de la Plata (RP), Kalahari (KAL), São Francisco-Congo (SFC), Borborema/Trans-Sahara block (BTS), Pará de Minas (PM).

plutonic mafic rocks of the Southern Espinhaço rift (1747–1700 Ma; *e.g.*, Silva 2016), as also to the tholeiitic mafic rocks of the Alto Rio Guanhães suite (1725 Ma). The magmatism related to the Espinhaço rift system (1790–1700 Ma; Suppl. Data A5) is also chrono-correlated to similar igneous assemblages recorded in the North China craton, as the Xiong'er volcanic rocks (1790–1745 Ma; Wang *et al.* 2016), the Taihang (1780 Ma; Peng 2015) and Miyun (1730 Ma; Peng 2015) dyke swarms, and also the volcanism related to the Yan-Liao rift (1730–1200 Ma; Peng 2015). The installation of the Xiong'er rift is chrono-correlated to the onset of the Espinhaço rift in the Early Statherian, while the development of the multiple stages of the Yan-Liao rift can be compared to the several taphrogenic events recorded from the Statherian to the Tonian-Cryogenian boundary in Espinhaço system region (Pedrosa-Soares and Alkmim 2011). However, as the record of Statherian magmatism are widely found in several other continental masses, like Amazonia, Baltica, Laurentia, Siberia, Australia, Antartica, Rio de La Plata (Ernst *et al.* 2013), paleomagnetic studies are necessary to better constrain these correlations and paleogeographic inferences.

The Espinhaço magmatism as a Silicic Large Igneous Province

According to the concept suggested by Bryan and Ernst (2008) and Ernst (2014), a Silicic Large Igneous Province (SLIP) presents the following five characteristics:

- the extrusive volume is greater than 0.25 Mkm^3 (up to > 3 Mkm^3) and the total exposure area larger than 0.1 Mkm^2;
- more than 80% of the province is represented by dacite–rhyolite, with transitional calc-alkaline I-type to A-type intraplate signature;
- rhyolitic ignimbrite is the predominant rock;
- the duration of magmatism is up to 40 Ma and shows a pulsed nature related to shorter intervals of 3 Ma to 10 Ma;
- the province is exclusively continental. The generation of such voluminous felsic magma is related to large degrees of partial melting of a hydrated, calc-alkaline, amphibolitic to andesitic lower continental crust (Bryan *et al.* 2002, Bryan and Ernst 2008).

In fact, the concept of Silicic Large Igneous Province (SLIP) was applied to the anorogenic magmatism related to the Statherian Espinhaço rift system by previous authors (Danderfer *et al.* 2015, Chaves *et al.* 2016), and it is now checked in the light of our data and compilation.

The present-day exposed crustal levels along the whole Espinhaço rift domains show rocks metamorphosed from the low greenschist to upper amphibolite facies, implying in the erosion of significant amounts of the Statherian volcanic rocks. Therefore, evaluations of the total volume and surface area once occupied by the overall Statherian anorogenic rocks are certainly underestimated. In this scenario, the Statherian Espinhaço magmatism is mostly characterized by metamorphosed, A-type, alkali-calcic to calc-alkalic granites, rhyolites, dacites, ignimbrites and acid volcaniclastic rocks, with continental intraplate signature (see references quoted in previous items). They represent more than 80% in exposed area of the whole Statherian igneous rocks and their metamorphosed equivalents. The mafic magmatism is very restricted, much probably representing less than 10% in area (Fig. 1).

Although spreading along a total area of more than 250.000 km^2, including the Espinhaço ridge, Chapada

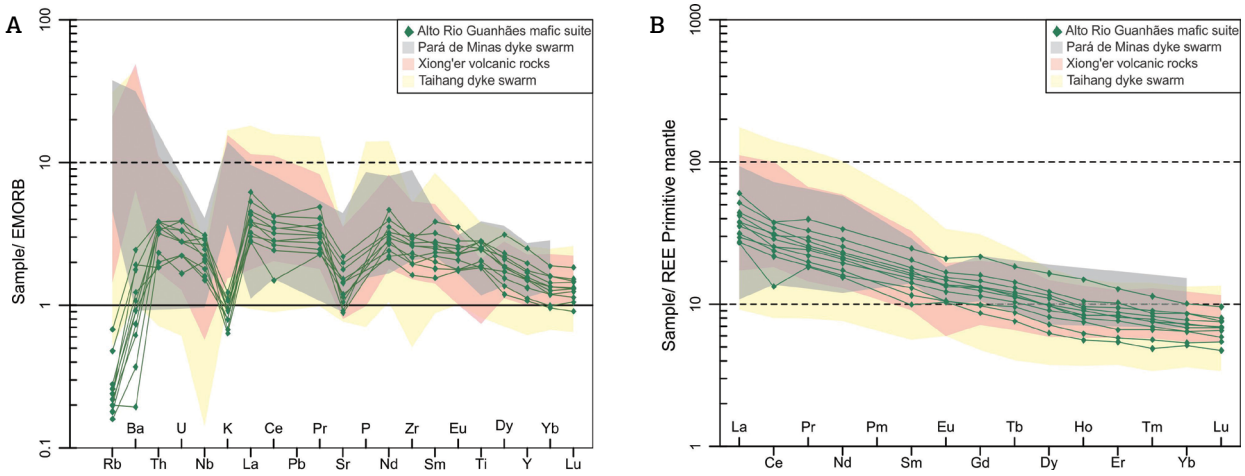

Figure 15. Trace element patterns of the Alto Rio Guanhães mafic suite (this study), Pará de Minas dyke swarm (Chaves 2001), the Xiong'er volcanic rocks (Zhao et al. 2002, Peng *et al.* 2008, He *et al.* 2009, Wang *et al.* 2010), the Taihang dykes (Hou *et al.* 2001, Peng *et al.* 2004, 2008, Peng 2015, Wang *et al.* 2004, 2007, 2008): (A) normalized to E-MORB; (B) normalized to Primitive Mantle. The normalization values are from Sun and McDonough (1989).

Diamantina and Guanhães block domains (Fig. 1), the occurrence areas of both felsic and mafic Statherian igneous rocks reach at least 70.000 km^2, because unknown parts of them are hidden beneath younger rock layers and extensive Cenozoic covers (Fig. 1). Although this surface area (> 70.000 km^2) is apparently smaller than the SLIP definition requirement (0.1 Mkm^2 or 100.000 km^2), it only shows the erosional remains found in present-day exposed crustal levels, most of them reworked within the Neoproterozoic Araçuaí orogen. Allowing to such exposure conditions, any evaluation of the original volume of extrusive rocks may be unreliable, although it can be expected a very large volume (possibly > 0.25 Mkm^3) of them, because the minimum area (> 70.000 km^2) and distribution of the present-day exposure areas of plutonic and volcanic felsic rocks are along more than 250.000 km^2 of relatively deep exposed crustal levels.

The high-quality U-Pb ages on zircons from the Statherian igneous rocks of the Espinhaço rift system span from 1792 ± 7 Ma to 1703 ± 12 Ma, with most values ranging from ca. 1752 Ma to ca. 1710 Ma (see Suppl. Data A5). This time interval (ca. 1752–1710 Ma) comprises at least 80% age values (almost all of them related to felsic rocks) of the dated Espinhaço igneous rocks, and is in good agreement with the maximum duration (ca. 40 Ma) suggested for a SLIP (cf. Bryan and Ernst 2008, Ernst 2014).

Therefore, bearing in mind the crustal level, exposed rocks and tectonic setting, the Espinhaço anorogenic province is, indeed, a good candidate to represent a SLIP, because it meets the main definition requirements, as the exclusive continental setting; the striking predominance of felsic (> 80% of A-type granites and rhyolites) over mafic (< 10%) rocks; a maximum duration of the felsic magmatism up to 40 Ma; and the very extensive, minimum total exposure area (despite the relatively deep erosional levels).

The data for the Alto Rio Guanhães mafic suite suggests a mantle upwelling beneath a stretched and thinned continental lithosphere, pointing to the involvement of the enriched lithospheric mantle in the generation of these rocks (Fig. 16). Although the trace elements pattern of this magmatism does not support a derivation from fertile sublithospheric composition, considering the life span of the Espinhaço anorogenic province, the contribution of fertile melts from a thermal anomaly (or mantle plume) can not be discarded.

As mentioned above (item 4.3.1), beyond the spatial- and chrono-correlation, the Alto Rio Guanhães mafic rocks display similar chemical characteristics with the Pará de Minas dyke swarm (Fig. 15) in the southern of the São Francisco craton. Therefore, these magmatic records can be either derived from a common parental magma or from a similar mantle source, suggesting they are part of the same igneous province.

CONCLUSION

- The volcanic mafic and felsic rocks interlayered on metasedimentary rocks of the Alto Rio Guanhães unit give new LA-ICPMS zircon U–Pb ages of 1725 ± 4 Ma and 1748 ± 3 Ma, respectively. The hornblende-biotite granite (Açucena pluton) of the Borrachudos suite yield SHRIMP zircon U–Pb age of 1740 ± 8 Ma, showing synchronicity between these magmatisms;
- The mafic rocks are all tholeiitic in compositions and are related to continental intraplate magmatism. They were

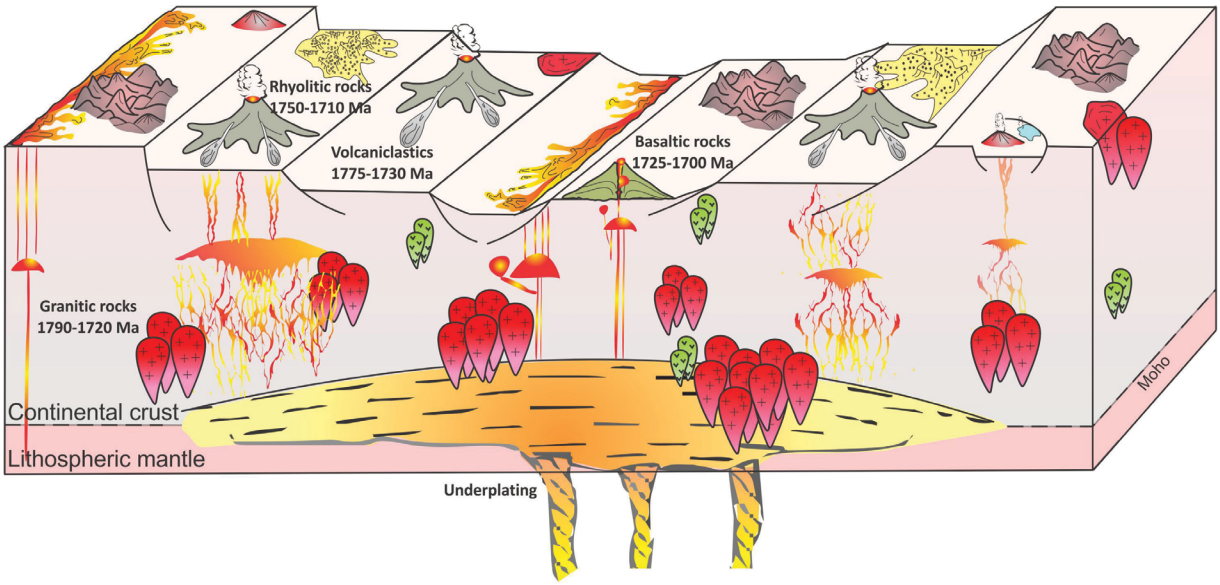

Figure 16. Schematic model for the Statherian magmatism related to the Espinhaço rift system.

most likely generated by melting of enriched subcontinental lithospheric mantle in the spinel-stable field and display the involvement of crustal assimilation accompanied by fractional crystallization processes in the generation of this magmatism. The anorogenic felsic magmatism may be derived by partial melting of Archean lower crustal materials by underplating of melts derived from the mantle;

- The Espinhaço rift system is characterized by a large volume of acid magmatism during its opening, whereas the mafic magmatism is only registered in the upper sequences of the Statherian rift system. Contrasting with the mafic rocks, so far restricted to the Southern and Central Espinhaço ranges and also the Guanhães block, the felsic rocks characterize a long-lived magmatism during the Statherian, with a ca. 1750–1710 Ma major magmatic event recorded throughout the whole Espinhaço rift system;
- Contemporaneous Statherian magmatism is reported elsewhere on the Southern São Francisco craton and, together with the Pará de Minas dyke swarm, the Alto Rio Guanhães rocks represent a rifting event;
- The main volumetric, compositional and tectonic parameters of the Espinhaço magmatism provide the evidence of a SLIP in the São Francisco and Congo paleocontinental blocks.

ACKNOWLEDGEMENT

The authors acknowledge the research financial support provided by the CNPq and CODEMIG. Joana Magalhães is grateful to the Brazilian Geological Survey (CPRM). Special thanks are given to Alexey Ulyanov for the assistance in the acquisition and reduction of trace elements in zircon data and to Katharina Marger for the assistance with $\delta^{18}O$ data acquisition.

SUPPLEMENTARY DATA

Supplementary data associated with this article can be found in the online version: Suplementary Table A1, Suplementary Table A2, Suplementary Table A3, Suplementary Table A4, Suplementary Table A5.

REFERENCES

Alkmim F.F. 2004. O que faz de um cráton um cráton? O Cráton do São Francisco e as revelações almeidianas ao delimita-lo. *In*: Mantesso-Neto V., Bartorelli A., Carneiro C.D.R., Brito Neves B.B. (eds.), *Geologia do Continente Sul-Americano:* evolução da obra de Fernando Flávio Marques de Almeida. Brasil, Beca, p. 17-35.

Alkmim F.F., Kuchenbecker M., Reis H.L.S., Pedrosa-Soares A.C. 2017. The Araçuaí Belt. *In*: Heilbron M., Cordani U.G., Alkmim F.F. (eds.), *São Francisco Craton, Eastern Brazil:* Tectonic Genealogy of a Miniature Continent. Cham, Springer, p. 255-276.

Alkmim F.F., Marshak S., Pedrosa-Soares A.C., Peres G.G., Cruz S.C.P., Whittington A. 2006. Kinematic evolution of the Aracuaí–West Congo orogen in Brazil and Africa: nutcracker tectonics during the Neoproterozoic assembly of Gondwana. *Precambrian Research*, **149**:43-64. dx.doi.org/10.1016/j.precamres.2006.06.007

Armstrong J.T. 1995. CITZAF - a package of correction programs for the quantitative electron microbeam X-ray analysis of thick polished materials, thin-films and particles. *Microbeam Analysis*, **4**(3):177-200.

Babinski M., Brito-Neves B.B., Machado N., Noce C.M., Uhlein A., Van Schmus W.R. 1994. Problemas da metodologia U-Pb em rochas vulcânicas continentais: Caso do Grupo Rio dos Remédios, Supergrupo Espinhaço, no Estado da Bahia. *In*: 38º Congresso Brasileiro de Geologia, Balneário Camboriú. *Anais*. v. 2, p. 409-410.

Barrote V.R. 2016. *A sequência portadora de formações ferríferas de Guanhães, Minas Gerais, Brasil.* MS Dissertation, Instituto de Geociências, Universidade Federal de Minas Gerais, Belo Horizonte, 134 p.

Bezerra-Neto F.E. 2016. *Estudo de rochas exóticas da formação sopa-brumadinho e possíveis implicações para a fonte dos diamantes do espinhaço meridional.* MS Dissertation, Instituto de Geociências, Universidade de Brasília, Brasília, 105 p.

Bindeman I. 2008. Oxygen isotopes in mantle and crustal magmas as revealed by single crystal analysis. *Reviews in Mineralogy and Geochemistry*, **69**(1):445-478. https://doi.org/10.2138/rmg.2008.69.12

Blevin P. 2003. Metallogeny of granitic rocks. *In*: The Ishihara Symposium, Granites and Associated Metallogenesis, Australia. *Short Papers*. v. 14, p. 5-8.

Brito-Neves B.B., Kawashita K., Cordani U.G., Delhal J. 1979. A evolução geocronológica da Cordilheira do Espinhaço - Dados Novos e Integração. *Revista Brasileira de Geociências*, **9**(1):71-85.

Bryan S.E., Ernst R.E. 2008. Revised definition of Large Igneous Provinces (LIPs). *Earth Science Reviews*, **86**(1-4):175-202. https://doi.org/10.1016/j.earscirev.2007.08.008

Bryan S.E., Riley T.R., Jerram D.A., Leat P.T., Stephens C.J. 2002. Silicic volcanism: an under-valued component of large igneous provinces and volcanic rifted margins. *In*: Menzies M.A., Klemperer S.L., Ebinger C.J., Baker J. (eds.), Magmatic Rifted Margins. Colorado, The Geological Society of America, Special Paper. p. 99-118.

Carvalho R.P., Rosière C.A., Rolim V.K., Lana C.C., Santos J.O.S. 2014. A sequência orosiriana-estateriana e geometria transpressiva na região de Santa Maria de Itabira, Minas Gerais. *Geologia USP. Série Científica*, **14**(2):111-120. https://doi.org/10.5327/Z1519-874X201400020006

Cederberg J., Söderlund U., Oliveira E.P., Ernst R.E., Pisarevsky S.A. 2016. U-Pb baddeleyite dating of the Proterozoic Pará de Minas dyke swarm in the São Francisco craton (Brazil) - implications for tectonic correlation with the Siberian, Congo and North China cratons. *GFF-Scandinavian Journal of Earth Sciences*, **138**:219-240. https://doi.org/10.1080/11035897.2015.1093543

Chaves A.O. 2001. *Enxames de diques máficos do Setor Sul do Cráton do São Francisco-MG*. PhD Thesis, Instituto de Geociências, Universidade de São Paulo, São Paulo, 165 p.

Chaves A.O., Fonseca W.M., Leal V.L.S. 2016. Províncias ígneas gigantes e o reposicionamento dos proto-crátons sul-americanos em Columbia na Transição Orosiriano-Estateriano. *Boletim do Museu Paraense Emílio Goeldi. Ciências Naturais*, **11**(2):263-280.

Chemale Jr. F. 1987. Gênese das rochas graníticas do tipo Borrachudos. In: 1º Congresso Brasileiro de Geoquímica, Porto Alegre. *Anais*. v. 1, p. 171-186.

Chemale Jr. F., Dussin I.A., Alkmim F.F., Martins M.S., Queiroga G.N., Armstrong R., Santos M.N. 2012a. Unravelling a Proterozoic basin history through detrital zircon geochronology: the case of the Espinhaço Supergroup, Minas Gerais, Brazil. *Gondwana Research*, **22**(1):200-206. http://dx.doi.org/10.1016/j.gr.2011.08.016

Chemale Jr. F., Kawashita K., Dussin I.A., Ávila J.N., Justino D., Bertotti A. 2012b. U-Pb zircon in situ dating with LA-MC-ICP-MS using a mixed detector configuration. *Anais da Academia Brasileira de Ciências*, **84**(2):275-295. http://dx.doi.org/10.1590/S0001-37652012005000032

Chu N.C., Taylor R.N., Chavagnac V., Nesbitt R.W., Boella R.M., Milton J.A., German C.A, Bayon G., Burton K. 2002. Hf isotope ratio analysis using multi-collector inductively coupled plasma mass spectrometry: an evaluation of isobaric interference corrections. *Journal of Analytical Atomic Spectrometry*, **17**(12):1567-1574. https://dx.doi.org/10.1039/B206707B

Compston W., Williams I.S., Kirschvink J.L., Zichao Z., Guogan M. 1992. Zircon ages for the Early Cambrian time-scale. *Journal of the Geological Society*, **149**:171-184. https://doi.org/10.1144/gsjgs.149.2.0171

Compston W., Williams I.S., Meyer C. 1984. U-Pb geochronology of zircons from the lunar breccia 73,217 using a sensitive high mass resolution ion microprobe. *Journal of Geophysical Research*, **89**(Supp. B):B525-B534. https://doi.org/10.1029/JB089iS02p0B525

Cordani U.G., Pimentel M.M., Ganade de Araújo C.E., Fuck R.A. 2013. The significance of the Transbrasiliano-Kandi tectonic corridor for the amalgamation of West Gondwana. *Brazilian Journal of Geology*, **43**(3):583-597. https://doi.org/10.5327/Z2317-48892013000300012

Costa A.F.O. 2013. *Estratigrafia e tectônica da borda oeste do Espinhaço Central no extremo norte da Faixa Araçuaí*. MS Dissertation, Departamento de Geologia/Escola de Minas, Universidade Federal de Ouro Preto, Ouro Preto, 170 p.

Costa A.F.O. 2017. Evolução tectono-estratigráfica da porção norte do Espinhaço Central, Norte de Minas Gerais. PhD Thesis, Departamento de Geologia/Escola de Minas, Universidade Federal de Ouro Preto, Ouro Preto, 220 p.

Cruz S.C.P., Alkmim F.F. 2017. The Paramirim Aulacogen. *In*: Heilbron M., Cordani U.G., Alkmim F.F. (eds.), *São Francisco Craton, Eastern Brazil:* Tectonic Genealogy of a Miniature Continent. Cham, Springer, p. 97-115.

D'Agrella-Filho M.S., Cordani U.G. 2017. The Paleomagnetic record of the São Francisco-Congo craton. *In*: Heilbron M., Cordani U.G., Alkmim F.F. (eds.), *São Francisco Craton, Eastern Brazil:* Tectonic Genealogy of a Miniature Continent. Cham, Springer, p. 305-320.

Danderfer A.F., Meireles H.P. 1987. *Mapeamento geológico da Região do Alto Rio Guanhães (MG)*. Trabalho de Graduação, Centro de Geologia Eschwege, Universidade Federal de Minas Gerais, Diamantina, 94 p.

Danderfer A., De Waele B., Pedreira A., Nalini Júnior H.A. 2009. New geochronological constraints on the geological evolution of Espinhaço basin within the São Francisco Craton-Brazil. *Precambrian Research*, **170**:116-128. dx.doi.org/10.1016/j.precamres.2009.01.002

Danderfer A., Lana C.C., Nalini Jr. H.A., Costa A.F.O. 2015. Constraints on the sthatherian Evolution of the intraplate rifting in a Paleo-Mesoproterozoic paleocontinent: New stratigraphic and geochronology record from the eastern São Francisco craton. *Gondwana Research*, **28**:668-688. http://dx.doi.org/10.1016%2Fj.gr.2014.06.012

DePaolo D.J. 1981. Trace element and isotopic effects of combined wallrock assimilation and fractional crystallization. *Earth and Planetary Science Letters*, **53**(2):189-202. https://doi.org/10.1016/0012-821X(81)90153-9

Dussin I.A. 2017. *Geocronologia U-Pb e Lu-Hf em zircão, Aplicada às Bacias Proterozóicas*. Estudo de Caso: Evolução Sedimentar e Tectônica da Bacia do Espinhaço – Setor Meridional, Minas Gerais, Brasil. Minas Gerais, Verlag-Novas Edições Acadêmicas, 124 p.

Dussin T.M. 1994. *Associacions vulcano- plutoniques de l'Espinhaço Meridional (SE - Brésil): un exemple d'évolution de la croûte protérozoïque*. PhD Thesis, Université D'Orléans, Orléans, 177 p.

Dussin T.M., Dussin I.A., Macambira M.J.B. 2000. Chronology of Mesoproterozoic Guanhães River sequence: 207Pb/206Pb single zircon evaporation data of metavolcanic rocks (Minas Gerais, Brazil). *In*: 31º Internacional Geolological Congress, Rio de Janeiro. *Abstracts*. CD-ROM.

Eby G.N. 1992. Chemical subdivision of the A-type granitoids: petrogenetic and tectonic implications. *Geology*, **20**:641-644. https://doi.org/10.1130/0091-7613(1992)020%3C0641:CSOTAT%3E2.3.CO;2

Ernst R.E. 2014. *Large igneous provinces*. Cambridge, Cambridge University Press, 667 p.

Ernst R.E., Pereira E., Hamilton M.A., Pisarevsky S.A., Rodrigues J., Tassinari C.C.G., Teixeira W., Van-Dunem V. 2013. Mesoproterozoic intraplate magmatic 'bar-code' record of the Angola portion of the Congo Craton: newly dated magmatic events at 1505 and 1110 Ma and implications for Nuna (Columbia) supercontinent reconstructions. *Precambrian Research*, **230**:103-118. https://doi.org/10.1016/j.precamres.2013.01.010

Fernandes M.L.S. 2001. *O Granito Borrachudos na região entre Guanhães e Dores de Guanhães, MG (Plutonito Morro do Urubu): gênese e evolução*. PhD Thesis, Instituto de Geociências, Universidade Federal de Minas Gerais, Belo Horizonte, 187 p.

Fernandes M.L.S., Marciano V.R.P.R.O., Oliveira R.C., Correia Neves J.M., Diláscio M.V. 1994. Granitos Borrachudos: um exemplo de granitogênese anorogênica na porção central do Estado de Minas Gerais. *Geonomos*, **2**(2):23-29. http://dx.doi.org/10.18285/geonomos.v2i2.223

Frost B.R., Barnes C.G., Collins W.J., Arculus R.J., Ellis D.J., Frost C.D. 2001. A geochemical classification for granitic rocks. *Journal of Petrology*, **42**(11):2033-2048. https://doi.org/10.1093/petrology/42.11.2033

Grimes C.B., John B.E., Kelemen P.B., Mazdab F.K., Wooden J.L., Cheadle M.J., Hanghøj K., Schwartz J.J. 2007. Trace element chemistry of zircons from oceanic crust: A method for distinguishing detrital zircon provenance. *Geology*, **35**(7):643-646. https://doi.org/10.1130/G23603A.1

Grossi Sad J.H., Chiodi Filho C., Santos J.F., Magalhães J.M.M., Carelos P.M. 1990. Duas suites graníticas do bordo sudeste do Craton São Francisco, em Minas Gerais: Petroquímica e Potencial Metalogenético. *In*: 36º Congresso Brasileiro de Geologia, Natal. *Anais*. v. 4, p. 1836-1841.

Guadagnin F., Chemale Jr. F., Magalhães A.J.C., Alessandretti L., Bállico M.B., Jeline A.R. 2015. Sedimentary petrology and detrital zircon U–Pb and Lu–Hf constraints of Mesoproterozoic intracratonic sequences in the Espinhaço Supergroup: Implications for the Archean and Proterozoic evolution of the São Francisco Craton. *Precambrian Research*, **266**:227-245. http://dx.doi.org/10.1016/j.precamres.2015.05.027

Harley S.L., Kelly N.M. 2007. The impact of zircon-garnet REE distribution data on the interpretation of zircon U-Pb ages in complex high-grade terrains: An example from the Rauer Islands, East Antarctica. *Chemical Geology*, **241**:62-87. https://doi.org/10.1016/j.chemgeo.2007.02.011

He Y., Zhao G., Sun M., Xia X. 2009. SHRIMP and LA-ICP-MS zircon geochronology of the Xiong'er volcanic rocks: implications for the Paleo-Mesoproterozoic evolution of the southern margin of the North China Craton. *Precambrian Research*, **168**(3-4):213-222. https://doi.org/10.1016/j.precamres.2008.09.011

Heilbron M., Cordani U.G., Alkmim F.F., Reis H.L. 2017. Tectonic Genealogy of a Miniature Continent. *In*: Heilbron M., Cordani U.G., Alkmim F.F. (eds.), *São Francisco Craton, Eastern Brazil:* Tectonic Genealogy of a Miniature Continent. Cham, Springer, p. 321-331.

Hoskin P.W., Schaltegger U. 2003. The composition of zircon and igneous and metamorphic petrogenesis. *Reviews in Mineralogy and Geochemistry*, **53**(1):27-62. https://doi.org/10.2113/0530027

Hou G.T., Li J.H., Qian X.L. 2001. Geochemical characteristics and tectonic setting of Mesoproterozoic dyke swarms in northern Shanxi. *Acta Petrologica Sinica*, **17**(3):352-357.

Hou G.T., Santosh M., Qian X.L., Lister G.S., Li J. 2008. Configuration of the Late Paleoproterozoic supercontinent Columbia: insights from radiating mafic dyke swarms. *Gondwana Research*, **14**(3):395-409. https://doi.org/10.1016/j.gr.2008.01.010

Humphris S.E., Thompson G., Schilling J.G., Kingsley R.H. 1985. Petrological and geochemical variations along the Mid-Atlantic Ridge between 46° S and 32° S: Influence of the Tristan da Cuhna mantle plume. *Geochimica et Cosmochimica Acta*, **49**:1445-1464. https://doi.org/10.1016/0016-7037(85)90294-7

Jackson S.E. 2008. LAMTRACE data reduction software for LA-ICP-MS. Laser ablation ICP-MS in the Earth sciences: current practices and outstanding issues. *Short Course Series*, Mineralogical Association of Canada, **40**:305-307.

Jackson S.E., Pearson N.J., Griffin W.L., Belousova E.A. 2004. The application of laser ablation-inductively coupled plasma-mass spectrometry to in situ U–Pb zircon geochronology. *Chemical Geology*, **211**(1-2):47-69. https://doi.org/10.1016/j.chemgeo.2004.06.017

Jaques A.L., Green D.H. 1980. Anhydrous melting of peridotite at 0-15 Kb pressure and the genesis of tholeiitic basalts. *Contributions to Mineralogy and Petrology*, **73**:287-310. https://doi.org/10.1007/BF00381447

Knauer L.G., Grossi-Sad J.H. 1997. Geologia da Folha Serro. *In*: Grossi-Sad J.H., Lobato L.M., Pedrosa-Soares A.C., Soares-Filho B.S. (eds.), *Projeto Espinhaço em CD-ROM (textos, mapas e anexos)*. Belo Horizonte, COMIG – Companhia Mineradora de Minas Gerais, p. 2057-2316.

Leake B.E., Wooley A., Arps C.E.S., Birch W.D., Gilbert M.C., Grice J.D., Hawthorne F.C., Kato A., Kisch H.J., Vladimir K., Linthout K., Laird J.O., Mandarino J.A., Maresch W.V., Nickel E.H., Rock N.M.S., Schumacher J.C., Smith D.C., Stephenson N.C.N., Ungaretti L., Whittaker E.J.W., Youzhi G. 1997. Nomenclature of amphiboles: report of the Subcommittee on Amphiboles of the International Mineralogical Association, Commission on New Minerals and Mineral Names. *American Mineralogist*, **82**:1019-1037.

Li X.H., Long W.G., Li Q.L., Liu Y., Zheng Y.F., Yang Y.H., Chamberlain K.R., Wan D.F., Guo C.H., Wang X.C., Tao H. 2010. Penglai zircon megacrysts: a potential new working reference material for microbeam determination of Hf–O isotopes and U–Pb age. *Geostandards and Geoanalytical Research*, **34**(2):117-134. https://doi.org/10.1111/j.1751-908X.2010.00036.x

Loiselle M.C., Wones D.R. 1979. Characteristic and origin of anorogenic granites. *Abstracts*, Geological Society of America, v. 11, p. 468.

Machado N., Schrank A., Abreu F.R., Knauer L.G, Almeida-Abreu P.A. 1989. Resultados preliminares da geocronologia U-Pb na Serra do Espinhaço Meridional. *In*: 5º Simpósio de Geologia de Minas Gerais, Belo Horizonte. *Anais*. v. 5, p. 171-174.

Martins-Neto M.A. 2000. Tectonics and sedimentation in a Paleo/Mesoproterozoic Rift-Sag Basin (Espinhaço Basin, southeastern Brazil). *Precambrian Research*, **103**:147-173.

McDonough W.F., Sun S.S. 1995. The composition of the Earth. *Chemical Geology*, **120**(3-4):223-253. https://doi.org/10.1016/0009-2541(94)00140-4

Moreira H.M. 2017. *Caracterização petrológica, geoquímica e geocronológica de corpos intrusivos máficos da Porção Central da Serra do Espinhaço*. MS Dissertation, Departamento de Geologia/Escola de Minas, Universidade Federal de Ouro Preto, Ouro Preto, 176 p.

Nelson D.R. 1997. *Compilation of SHRIMP U–Pb zircon geochronology data*. Geological Survey of Western Australia, Record, 242 p.

Noce C.M., Pedrosa-Soares A.C., Silva L.C., Alkmim F.F. 2007a. O embasamento arqueano e paleoproterozóico do Orógeno Araçuaí. *Genomos*, **15**(1):17-23. http://dx.doi.org/10.18285/geonomos.v15i1.104

Noce C.M., Pedrosa-Soares A.C., Silva L.C., Armstrong R., Piuzana D. 2007b. Evolution of polycyclic basement complexes in the Araçuaí Orogen, based on U–Pb SHRIMP data: Implications for Brazil–Africa links in Paleoproterozoic time. *Precambrian Research*, **159**(1-2):60-78. http://ib.adnxs.com/seg?add=1&redir=http%3A%2F%2Fdx.doi.org%2F10.1016%2Fj.precamres.2007.06.001

Oliveira A.A.K. 2002. *Estruturação e alteração metassomática do ortognaisse Açucena (suíte borrachudos) na região de Ipatinga, Minas Gerais*. MS Dissertation, Instituto de Geociências, Universidade Federal de Minas Gerais, Belo Horizonte, 98 p.

Patchett P.J., Tatsumoto M. 1981. A routine high-precision method for Lu-Hf isotope geochemistry and chronology. *Contributions to Mineralogy and Petrology*, **75**(3):263-267. https://doi.org/10.1007/BF01166766

Pearce J.A. 2008. Geochemical fingerprinting of oceanic basalts with applications to ophiolite classification and the search for Archean oceanic crust. *Lithos*, **100**(1-4):14-48. https://doi.org/10.1016/j.lithos.2007.06.016

Pearce J.A., Harris N.B.W., Tindle A.G., 1984. Trace element discrimination diagrams for the tectonic interpretation of granitic rocks. *Journal of Petrology*, **25**:956-983.

Pearce J.A., Norry M.J. 1979. Petrogenetic implications of Ti, Zr, Y, and Nb variations in volcanic rocks. *Contributions to Mineralogy and Petrology*, **69**(1):33-47. https://doi.org/10.1007/BF00375192

Peccerillo A., Barberio M.R., Yirgu G., Ayalew D., Barbieri M., Wu T.W. 2003. Relationships between mafic and peralkaline felsic magmatism in continental rift settings: a petrological, geochemical and isotopic study of the Gedemsa Volcano, Central Ethiopian Rift. *Journal of Petrology*, **44**:2003-2032. https://doi.org/10.1093/petrology/egg068

Pedrosa-Soares A.C., Alkmim F.F. 2011. How many rifting events preceded the development of the Araçuaí-West Congo orogeny? *Geonomos*, **19**(2):244-251. http://dx.doi.org/10.18285/geonomos.v19i2.56

Pedrosa-Soares A.C., Alkmim F.F., Tack L., Noc C.M., Babinski M., Silva L.C.D., Martins-Neto M.A. 2008. Similarities and differences between the Brazilian and African counterparts of the Neoproterozoic Araçuaí-West Congo orogen. *Geological Society of London Special Publication*, London, **294**(1):153-172.

Pedrosa-Soares A.C., Campos C.P., Noce C., Silva L.C., Novo T., Roncato J., Medeiros S., Castañeda C., Queiroga G., Dantas E., Dussin I., Alkmim F.F. 2011. Late Neoproterozoic-Cambrian granitic magmatism in the Araçuaí orogen (Brazil), the Eastern Brazilian Pegmatite Province and related mineral resources. *In*: Sial A.N., Bettencourt J.S., De Campos C.P., Ferreira V.P. (eds), *Granite-Related Ore Deposits*. London, Geological Society of London Special Publication, 350, p. 25-51.

Peixoto E., Pedrosa-Soares A.C., Alkmim F.F., Dussin I.A. 2015. A suture–related accretionary wedge formed in the Neoproterozoic Araçuaí orogen (SE Brazil) during Western Gondwanaland assembly. *Gondwana Research*, **27**(2):878-896. http://dx.doi.org/10.1016/j.gr.2013.11.010

Peng P. 2015. Precambrian mafic dyke swarms in the North China Craton and their geological implications. *Science China Earth Sciences*, **58**(5):649-675. https://doi.org/10.1007/s11430-014-5026-x

Peng P., Zhai M., Ernst R.E., Guo J., Liu F., Hu B. 2008. A 1.78 Ga large igneous province in the North China craton: the Xiong'er Volcanic Province and the North China dyke swarm. *Lithos*, **101**(3-4):260-280. https://doi.org/10.1016/j.lithos.2007.07.006

Peng P., Zhai M., Zhang H., Zhao T., Ni Z. 2004. Geochemistry and Geological Significance of the 1.8 Ga Mafic Dyke Swarms in the North China craton: an Example from the Juncture of Shanxi, Hebei and Inner–Mongolia. *Acta Petrologica Sinica*, **20**:439-456.

Pimentel M.M., Heaman L.M., Fuck R.A., Marini O.J. 1991. U–Pb zircon geochronology of Precambrian tin-bearing continental-type acid magmatism in central Brazil. *Precambrian Research*, **52**:321-335. https://doi.org/10.1016/0301-9268(91)90086-P

Pimentel M.M., Machado N., Lobato L.M. 1994. Geocronologia U/Pb de rochas graníticas e gnáissicas da região de Lagoa Real, Bahia, e implicações para a idade da mineralização de urânio. *In*: 38º Congresso Brasileiro de Geologia, Balneário Camboriú. *Boletim*, p. 389-390.

Pinto C.P., Silva M.A. 2014. *Mapa Geológico do Estado de Minas Gerais, Brasil*. Escala 1:1.000.000. Belo Horizonte, CODEMIG – Companhia de Desenvolvimento Econômico de Minas Gerais; CPRM – Companhia de Pesquisa de Recursos Minerais.

Rogers J.J.W. 1996. A history of continents in the past three billion years. *Journal of Geology*, **104**(1):91-107.

Rogers J.J.W., Santosh M. 2002. Configuration of Columbia, a Mesoproterozoic supercontinent. *Gondwana Research*, **5**:5-22. https://doi.org/10.1016/S1342-937X(05)70883-2

Rolim V.K., Rosière C.A., Santos J.O.S., McNaughton N.J. 2016. The Orosirian-Statherian banded iron formation-bearing sequences of the southern border of the Espinhaço Range, Southeast Brazil. *Journal of South American Earth Sciences*, **65**:43-66. http://doi.org/10.1016/j.jsames.2015.11.003

Rollinson H. 1993. *Using geochemical data:* evaluation, presentation, interpretation. New York, Longman Scientific, 352 p.

Rubatto D. 2017. Zircon: the metamorphic mineral. *Reviews in Mineralogy and Geochemistry*, **83**(1):261-295. https://doi.org/10.2138/rmg.2017.83.9

Santos M.N., Chemale Jr. F., Dussin I.A., Martins M., Assis T.A.R., Jelinek A.R., Guadagnin F., Armstrong R. 2013. Sedimentological and paleoenvironmental constraints of the Statherian and Stenian Espinhaço rift system, Brazil. *Sedimentary Geology*, **290**:47-59. https://doi.org/10.1016/j.sedgeo.2013.03.002

Schobbenhaus C., Hoppe A., Baumann A., Lork A. 1994. Idade U/Pb do vulcanismo Rio dos Remédios, Chapada Diamantina, Bahia. *In*: 38º Congresso Brasileiro de Geologia, Balneário Camboriú. *Boletim*, p. 397-399.

Shand S.J. 1943. *Eruptive Rocks*. Their Genesis, Composition, Classification, and Their Relation to Ore-Deposits with a Chapter on Meteorite. New York, John Wiley & Sons, 350 p.

Silva L.C., Pedrosa-Soares A.C., Armstrong R., Noce M.R. 2011. Determinando a duração do período colisional do Orógeno Araçuaí com base em geocronologia U-Pb de alta resolução em zircão: uma contribuição para a história da amalgamação do Gondwana Ocidental. *Geonomos*, **19**(2):180-197. http://dx.doi.org/10.18285/geonomos.v19i2.53

Silva L.C., Pedrosa-Soares A.C., Armstrong R., Pinto C.P., Magalhães J.T.R., Pinheiro M.A.P., Santos G.G. 2016. Disclosing the Paleoarchean to Ediacaran history of the São Francisco craton basement: The Porteirinha domain (northern Araçuaí orogen, Brazil). *Journal of South American Earth Sciences*, **68**:50-67. http://dx.doi.org/10.1016/j.jsames.2015.12.002

Silva M.C.R. 2016. *A Formação Sopa-Brumadinho nos campos diamantíferos de São João da Chapada, Sopa-Guinda e Extração, Diamantina-Minas Geraisurânio-chumbo e isótopos de háfnio: sistemas deposicionais, tratos de sistemas, geoquímica e geocronologia urânio-chumbo e isótopos de háfnio*. PhD Thesis, Instituto de Geociências, Universidade Federal de Minas Gerais, Belo Horizonte, 335 p.

Silveira-Braga F.C. 2012. *A sequência portadora de formação ferrífera da Serra do Morro Escuro, Santa Maria de Itabira, Minas Gerais*. MS Dissertation, Instituto de Geociências, Universidade Federal de Minas Gerais, Belo Horizonte, 299 p.

Silveira-Braga F.C., Rosière C.A., Queiroga G.N., Rolim V.K., Santos J.O.S., McNaughton N.J. 2015. The Statherian itabirite-bearing sequence from the Morro Escuro Ridge, Santa Maria de Itabira, Minas Gerais, Brazil. *Journal of South American Earth Sciences*, **58**:33-53. http://dx.doi.org/10.1016/j.jsames.2014.12.004

Soares-Filho B.S. 1987. *Mapeamento regional*. Projeto Ouro Fino-Conceição do Mato Dentro. METAMIG, Relatório Interno. Belo Horizonte, METAMIG.

Sun S.S. 1980. Lead isotopic study of young volcanic rocks from mid-ocean ridges, ocean islands and island arcs. *Philosophical Transactions of the Royal Society of London*, **297**:409-445. http://dx.doi.org/10.1098/rsta.1980.0224

Sun S.S., McDonough W.F. 1989. Chemical and isotopic systematics of oceanic basalts: implications for mantle composition and processes. *In*: Saunders A.D., Norry M.J. (eds), *Magmatism in the ocean basins*. London, Geological Society of London Special Publication, 42, p. 313-345.

Taylor S.R., McLennan S.M. 1985. *The continental crust:* its composition and evolution. Oxford, Blackwell Scientific Publications, 312 p.

Teixeira W., Oliveira E.P., Peng P., Dantas E.L., Hollanda M.H. 2017. U-Pb geochronology of the 2.0 Ga Itapecerica graphite-rich supracrustal succession in the São Francisco Craton: Tectonic matches with the North China Craton and paleogeographic inferences. *Precambrian Research*, **293**:91-111.

Turpin L., Maruejol P., Cuney M. 1988. U-Pb, Rb-Sr and Sm-Nd chronology of granitic basement, hydrotermal albitites and uranium mineralization, Lagoa Real, South Bahia, Brazil. *Contribution to Mineralogy and Petrology*, **98**:139-147. https://doi.org/10.1007/BF00402107

Valley J.W. 2003. Oxygen isotopes in zircon. *Reviews in Mineralogy and Geochemistry*, **53**(1):343-385. https://doi.org/10.2113/0530343

Valley J.W., Kinny P.D., Schulze D.J., Spicuzza M.J. 1998. Zircon megacrysts from kimberlite: oxygen isotope variability among mantle melts. *Contributions to Mineralogy and Petrology*, **133**(1-2):1-11. https://doi.org/10.1007/s004100050432

Valley J.W., Lackey J.S., Cavosie A.J., Clechenko C.C., Spicuzza M.J., Basei M.A.S., Bindeman I.N., Ferreira V.P., Sial A.N., King E.M., Peck W.H., Sinha A.K., Wei C.S., Peck W.H. 2005. 4.4 billion years of crustal maturation: oxygen isotope ratios of magmatic zircon. *Contributions to Mineralogy and Petrology*, **150**(6):561-580. https://doi.org/10.1007/s00410-005-0025-8

Xu H., Yang Z., Peng P., Ge K., Jin Z., Zhu R. 2017. Magnetic fabrics and rock magnetism of the Xiong'er volcanic rocks and their implications for tectonic correlation of the North China Craton with other crustal blocks in the Nuna/Columbia supercontinent. *Tectonophysics*, **712**:415-425. http://dx.doi.org/10.1016/j.tecto.2017.06.015

Wang C., Lu Y., He X., Wang Q., Zhang J. 2016. The Paleoproterozoic diorite dykes in the southern margin of the North China Craton: Insight into rift-related magmatism. *Precambrian Research*, **277**:26-46. https://doi.org/10.1016/j.precamres.2016.02.009

Wang K., Plank T., Walker J.D., Smith E.I. 2002. A mantle melting profile across the Basin and Range, SW USA. *Journal of Geophysical Research: Solid Earth*, **107**(B1):21. https://doi.org/10.1029/2001JB000209

Wang X.L., Jiang S.Y., Dai B.Z. 2010. Melting of enriched Archean subcontinental lithospheric mantle: Evidence from the ca. 1760 Ma volcanic rocks of the Xiong'er Group, southern margin of the North China Craton. *Precambrian Research*, **182**(3):204-216. https://doi.org/10.1016/j.precamres.2010.08.007

Wang Y.J., Fan W.M., Zhang Y.H., Guo F., Zhang H.F., Peng T.P. 2004. Geochemical, 40Ar/39Ar geochronological and Sr–Nd isotopic constraints on the origin of Paleoproterozoic mafic dikes from the southern Taihang Mountains and implications for the ca. 1800 Ma event of the North China craton. *Precambrian Research*, **135**:55-77. https://doi.org/10.1016/j.precamres.2004.07.005

Wang Y.J., Zhao G.C., Cawood P.A., Fan W.M., Peng T.P., Sun L.H. 2008. Geochemistry of Paleoproterozoic (~1770 Ma) mafic dykes from the Trans-North China Orogen and tectonic implications. *Journal of Asian Earth Sciences*, **33**:61-77. http://dx.doi.org/10.1016/j.jseaes.2007.10.018

Wang Y.J., Zhao G.C., Fan W.M., Peng T.P., Sun L.H., Xia X. 2007. LA–ICP–MS U Pb zircon geochronology and geochemistry of Paleoproterozoic mafic dykes from western Shandong Province: implications for back-arc basin magmatism in the Eastern Block, North China Craton. *Precambrian Research*, **154**:107-124. http://dx.doi.org/10.1016/j.precamres.2006.12.010

Whalen J.B., Currie K.L., Chappell B.W. 1987. A-type granites: geochemical characteristics, discrimination and petrogenesis. *Contributions to Mineralogy and Petrology*, **95**:407-419. https://doi.org/10.1007/BF00402202

Wiedenbeck M., Allé P., Corfu F., Griffin W.L., Meier M., Oberli F., Von Quadt A., Roddick J.C., Spiegel W. 1995. Three natural zircon standards for U-Th-Pb, Lu-Hf, trace element and REE analyses. *Geostandards Newsletter*, **19**:1-23. https://doi.org/10.1111/j.1751-908X.1995.tb00147.x

Wilson B.M. 2007. *Igneous petrogenesis, a global tectonic approach*. Dordrecht, Springer Science & Business Media, 466 p.

Wood D.A. 1980. The application of a Th-Hf-Ta diagram to problems of tectonomagmatic classification and to establish the nature of crustal contamination of basaltic lavas of the British Tertiary volcanic province. *Earth and Planetary Science Letters*, **50**:11-30. https://doi.org/10.1016/0012-821X(80)90116-8

Zhao G., Sun M., Wilde S.A., Li S. 2004. A Paleo-Mesoproterozoic supercontinent: assembly, growth and breakup. *Earth-Science Reviews*, **67**(1-2):91-123. https://doi.org/10.1016/j.earscirev.2004.02.003

Zhao T.P., Zhou M.F., Zhai M., Xia B. 2002. Paleoproterozoic rift-related volcanism of the Xiong'er Group, North China craton: implications for the breakup of Columbia. *International Geology Review*, **44**(4):336-351. https://doi.org/10.2747/0020-6814.44.4.336

APPENDIX A. ANALYTICAL METHODS.

A1. Mineral chemical compositions

Polished sections were analyzed for in situ mineral chemistry in a JEOL JXA-8200 Superprobe at the Institute of Earth Sciences, University of Lausanne, Switzerland, using a 15 kV accelerating voltage, 20 nA beam current and 3–5 μm beam diameter. Counting times were 20s on peak and 10s on background. Natural silicates and oxides from the laboratory collection were used as standards for calibration. Repeated measurements of standards at the start of each analytical session gave precisions < 2% for analysed oxides. The phi–rho–Z matrix correction method was applied (Armstrong 1995). Results are reported in Supplementary Data 1.

A2. Whole rock major and trace elements

Major, trace and rare earth elements analyses on 12 selected samples were conducted by ACME Analytical Laboratories Ltd., Canada. The analyses were performed via ICP-MS after fusion with lithium metaborate/tetraborate and digestion with diluted nitric acid, with analytical errors of 5% for most of the major oxides and 10–15% for most of the trace and rare earth elements. Base and precious metal grades were determined by digestion in Aqua Regia. The analyses were performed by Inductively Coupled Plasma-Atomic Emission Spectrometry (ICP-AES) for major elements, whilst trace elements have been determined by Inductively Coupled Plasma-Mass Spectrometry (ICP-MS), according to their specific routines. Results are reported in Supplementary Data 2.

A3. Zircon U–Pb LA-ICPMS dating

The in situ zircon U-Pb LA-ICPMS dating analyses reported here were carried out using an ArF Excimer Laser 193 nm - ATLEX (Photon, Machines Inc.) laser-ablation microprobe, coupled to a Neptune-Plus Plasma multi-collector (Thermo Fisher Scientific), at the MULTILAB Laboratory, University of Rio de Janeiro State, Brazil. Zircons were mounted in epoxy, with 2.5 cm in diameter and 0.5 mm height, and polished before being imaged by the cathodoluminescence Quanta-250-FEI. Isotopic data were acquired by the static mode and 25 μm beam size. Instrument set up parameters were 8–9 mJ/cm^2 laser fluency, 10 Hz, 25 μm and laser energy spot between 20 and 40%. Fraction of elements by laser induction and mass instrumental discrimination were corrected using the reference standard of zircon GJ-1 (Jackson *et al.* 2004) as primary standard and tested using the zircon 91500 (Wiedenbeck *et al.* 1995). External errors were calculated with the error spread of individual measurements of GJ-1 standard and individual measurements of each zircon sample (or spot), according to Chemale Jr. *et al.* (2012b). Results are reported in Supplementary Data 3.

A4. Zircon U–Pb SHRIMP dating

The isotopic U–Pb SHRIMP analyses were obtained at the SHRIMP II equipment at the Australia National University, Australia. About 100 crystals were selected and then cast in a standard 25-mm epoxy mount and sectioned by polishing. All the dated crystals had cathodoluminescence (CL) images done before the SHRIMP analyses. Instrumental conditions and data acquisition have been described in Compston *et al.* (1984, 1992). The SHRIMP operation and particular procedures followed the usual routine described by Nelson (1997). The Pb, U and Th concentrations were referenced to the standard zircon. One determination on the standard was obtained for each three analyses on the unknown. The spot size is typically 25 μm in diameter. The age uncertainties given in the text are at the 95% confidence level for the concordant populations, and the internal precision for single analyses in the table is 1σ. Results are reported in Supplementary Data 3.

A5. In situ zircon Hf isotopic analyses

Hf isotopes were obtained via Laser Ablation Multicollector Inductively Coupled Plasma Mass Spectrometry (NdYAG 193nm Photon Machine / Neptune Thermo Scientific) at the Isotope Geochemistry Laboratory, Federal University of Rio Grande do Sul, Brazil. Data were collected in static mode during 60s of ablation with a spot size of 50 μm. Nitrogen (~ 0.080 l/min) was introduced into the Ar sample carrier gas. Typical signal intensity was ca. 12 V for ^{180}Hf. The isotopes ^{172}Yb, ^{173}Yb and ^{175}Lu were simultaneously monitored during each analysis step to allow for correction of isobaric interferences of Lu and Yb isotopes on mass 176. The ^{176}Yb and ^{176}Lu were calculated using a ^{176}Yb/^{173}Yb of 0.796218 (Chu *et al.* 2002) and ^{176}Lu/^{175}Lu of 0.02658 (JWG in-house value). The correction for instrumental mass bias utilized an exponential law and ^{179}Hf/^{177}Hf value of 0.7325 (Patchett and Tatsumoto 1981) for correction of Hf isotopic ratios. The mass bias of Yb isotopes generally differs slightly from that of the Hf isotopes with a typical offset of the βHf/βYb of ca. 1.04 to 1.06 when using the ^{172}Yb/^{173}Yb value of 1.35274 from Chu *et al.* (2002). This offset was determined for each analytical session by averaging the βHf/βYb of multiple analyses of the JMC 475 solution doped with variable Yb amounts and all laser ablation analyses (typically n > 50) of TEMORA zircon with a ^{173}Yb signal intensity of > 60 mV. The mass bias behavior of Lu was assumed to follow that of Yb. The Yb and Lu isotopic ratios were corrected using the βHf of the individual integration steps of each analysis

divided by the average offset factor of the complete analytical session. Results are reported in Supplementary Data 4.

A6. In situ zircon oxygen isotopic analysis

$^{18}O/^{16}O$ ratios on zircons were measured using a Cameca IMS 1280HR ion probe at the SwissSIMS facility, University of Lausanne, Switzerland. The measurements were made with a focused 10kV Cs^+ beam with an intensity of about 2 nA current and a 15 µm rastered spot size. Each analysis took ca. 4 min, including pre-sputtering (60 s). Oxygen isotopes were analyzed at a multi-collector mode using Faraday cups. Mass calibration was performed at the beginning of the session. The instrumental mass fractionation factor (IMF) was corrected using the Plengai zircon international standard (Li *et al*. 2010). Four analyses of the standard were performed routinely at the beginning of the session, and subsequently after every 13 unknowns. Errors reported for each sample are the 2SD of the instrumental mass fractionation factor. The reproducibility for the Plengai zircon averaged 0.3% (2SD) and the variations over the entire session were between 0.18 and 0.37% (2SD). Following analyses, all ion microprobe spots were reexamined by Scanning Electron Microscopy (SEM). Results are reported in Supplementary Data 4.

A7. In situ zircon trace elements

Trace element analyses on zircons were conducted by LA-ICP-MS, the sector-field spectrometer Element XR interfaced to a NewWave UP-193 ArF excimer ablation system at the Institute of Earth Sciences, University of Lausanne, Switzerland. A beam size of 35 µm at 10 Hz was used. The NIST SRM 612 glass was used as the reference material and measured twice at the beginning and at the end of the analytical sequence of 12 unknowns. Background and ablation interval acquisition times were about 100 and 50 s, respectively. Dwell times range from 10 to 20ms. LAMTRACE software (Jackson 2008) was used for data reduction assuming SiO_2 = 31.57 wt% for zircon. The trace element analyses spots were placed near the U-Pb dating and Lu-Hf spots considering the same CL-domains. Results are reported in Supplementary Data 4.